Robotica (2018) volume 36, pp. 374–394. © Cambridge University Press 2017
doi:10.1017/S0263574717000455

Three-dimensional tracking control of autonomous underwater vehicles with limited torque and without velocity sensors

Khoshnam Shojaei*

Department of Electrical Engineering, Najafabad Branch, Islamic Azad University, Najafabad, Iran

(Accepted October 7, 2017. First published online: November 16, 2017)

SUMMARY

Most of the previous works on the motion control of autonomous underwater vehicles (AUVs) assume that (i) the vehicle actuators are able to tolerate every level of the control signals, and (ii) the vehicle is equipped with the velocity sensors in all degrees of freedom. These assumptions are not desirable in practice. Toward this end, this paper addresses the trajectory tracking control of the underactuated AUVs with the limited torque, without the velocity measurements and under environmental disturbances in a three-dimensional space. At first, a variable transformation is introduced which helps us to derive a second-order dynamic model for underactuated AUVs. Then, a saturated tracking controller is proposed by employing the saturation functions to bound the closed-loop error variables. This technique reduces the risk of the actuators saturation by decreasing the amplitude of the generated control signals. In addition, a nonlinear saturated observer is introduced to remove the velocity sensors from the control system. The proposed controller copes with the uncertain vehicle parameters, and constant or time-varying environmental disturbances induced by the waves and ocean currents. Lyapunov's direct method is used to show the semi-global uniform ultimate boundedness of the tracking and state estimation errors. Finally, some simulation results illustrate the effectiveness of the proposed controller.

KEYWORDS: Actuator saturation, Autonomous underwater vehicles, Adaptive control, Output feedback, Trajectory tracking

1. Introduction

1.1. Background and related works

The motion control of the underactuated autonomous underwater vehicles (AUVs) has been extensively studied from the control, robotic and ocean engineering communities over recent years. This interest essentially originates from a wide range of the applications of such vehicles including search, surveillance, rescue operations, exploration, reconnaissance, oceanographic mapping, geological sampling, ocean floor survey, mine-sweeping and deep sea archaeology. The interested readers are referred to the survey paper[1] and references therein for an introduction to the design and control of such systems. In contrast to the motion control of fully-actuated AUVs, the main concern in the design of controllers for underactuated ones is that the number of their independent actuators is fewer than the degrees of freedom. This limitation may be due to the mechanical or electrical failures of actuators during an operation. Sometimes, a deliberate reduction in the number of actuators is considered to decrease the weight and cost of the system. This feature, in turn, increases the degree of complexity in the design of nonlinear tracking controllers for such vehicles.

Seminal works on the motion control of underactuated AUVs have been reported in refs. [2]–[4] which the AUV dynamic model is neglected. Motivated by the challenging nature of the motion control problems of underactuated AUVs and their offshore applications, many research works

* Corresponding author. E-mail: khoshnam.shojaee@gmail.com

have been reported to solve the stabilization,[5–7] homing,[8] path-following,[9,10] way-point tracking,[11] trajectory tracking,[12,13] output feedback (OFB)[14,15] control of underactuated AUVs. In refs. [11]–[13], tracking controllers are proposed for underactuated AUVs by using a 3-degree-of-freedom (DOF) model. However, the velocity measurements are necessary to be available for the feedback and all results are presented for the planar motion. In spite of extensive researches, most of the previous controllers[1–13] need velocity measurements for real implementations. Since velocity sensors may increase the cost of real implementations and the weight of the system, their application is not desirable in practice. One reasonable solution to omit the velocity sensors is the design of OFB controllers by utilizing the velocity observers. However, since the separation principle in the design of the observer-based controllers is not applicable for nonlinear systems such as AUVs, the design of an output feedback controller (OFBC) is still a challenging task in current researches. The design of OFBCs may be even more difficult in the presence of parametric uncertainties, unmodeled dynamics and environmental disturbances in AUVs model. To address this problem, Do *et al.*[14] proposed a global OFBC for an underactuated AUV. However, their proposed controller cannot overcome the imprecise knowledge of the AUV parameters. Refsnes *et al.*[15] proposed a model-based OFBC for the slender-body underactuated AUVs which needs model parameters for the implementation of the observer-based controller. Subudhi *et al.*[16] proposed a static output feedback OFBC for the path following of AUVs in the vertical plane by using Serret–Frenet frame. Unfortunately, the proposed controllers in refs. [14]–[16] neglect the actuators saturation.

Recently, different motion control problems have been addressed for AUVs in the literature.[17–20] However, the main shortcoming of all previous works[2–20] is that they assume that AUV actuators are capable of tolerating every level of input signals and they generate the necessary level of the torque signals. However, the large amplitudes of generated control signals may force the actuators to go beyond their natural capabilities which may lead to their saturation in practical situations. The actuator saturation is not desirable in practice and it may deteriorate the tracking performance of the proposed controller especially in the transient response. In addition, a long-term saturation may lead to thermal, electrical or mechanical failures of the actuators. One solution to improve this situation is bounding of the closed-loop error variables by applying a saturation function in the design of the tracking controller. This paper addresses the above mentioned problems for the AUVs.

1.2. Contributions of this paper

According to the best of the author's knowledge, the trajectory tracking control problem of underactuated AUVs with saturating actuators and without velocity sensors has not been addressed in the available literature. This paper proposes a saturated OFB tracking controller to solve this problem in the three-dimensional (3D) space for the first time. For this purpose, a variable transformation is introduced based on a 5-DOF AUV model which includes all posture variables to incorporate the AUV dynamics in all directions and to involve all control inputs. This transformation helps us to derive a new second-order formulation for the AUV model. Then, a saturated observer-based tracking controller is proposed to stabilize underactuated AUVs towards desired trajectories. The following contributions are taken into account in this paper with respect to the previous works:

(i) Saturation functions will be employed to bound the tracking and state estimation errors in the design of the controller and velocity observer. This technique reduces the risk of the actuator saturation and consequently improves the transient response of the control system.
(ii) A nonlinear saturated observer is introduced to estimate the AUV velocities in the surge, pitch and yaw directions. The observer design and the assumption of the passive-boundedness of the sway and heave velocities play key roles to leave out velocity sensors for the implementation of the proposed controller.
(iii) According to the literature,[1–22] there exist a few works to solve the tracking control problem of underactuated AUV in a 3D space. This paper addresses this problem by utilizing a coordinate transformation for a 5-DOF AUV model.
(iv) Since AUV parameters such as the mass, inertia and damping coefficients are difficult to be obtained accurately[10] and the environmental disturbances are unavoidable due to waves, wind and ocean currents, an adaptive saturation-type controller is also adopted for the robustness of the proposed controller.

https://doi.org/10.1017/S0263574717000455 Published online by Cambridge University Press

The rest of this paper is organized as follows: The problem formulation is presented in the next section. A variable transformation is introduced to develop a second-order model of AUVs which plays a key role in the design of the controller. In Section 3, a saturated OFB control system is proposed and its Lyapunov-based stability analysis is presented. In Section 4, simulation results are provided to show the effectiveness of the proposed controller. Conclusions are given in Section 5.

2. Problem Formulation

2.1. Notations

Throughout this paper, $\|\boldsymbol{x}\| := \sqrt{\boldsymbol{x}^T\boldsymbol{x}}$ is used to show Euclidean norm of a vector $\boldsymbol{x} \in \Re^n$, whereas the norm of a matrix $\boldsymbol{A}$ is defined by the induced norm, i.e. $\|\boldsymbol{A}\| := \sqrt{\lambda_{\max}(\boldsymbol{A}^T\boldsymbol{A})}$. The term $\lambda_{\max}(\bullet)$ ($\lambda_{\min}(\bullet)$) represents the largest (smallest) eigenvalue of a matrix. The matrix $\boldsymbol{I}_n$ denotes an n-dimensional identity matrix. To simplify the subsequent control design and its stability analysis, the notations $\boldsymbol{Tanh}(\boldsymbol{\eta}) := [\tanh(\eta_1), \tanh(\eta_2), \ldots, \tanh(\eta_n)]^T$ and $\boldsymbol{Sech}^2(\boldsymbol{\eta}) = \mathrm{diag}[\mathrm{sech}^2(\eta_1), \ldots, \mathrm{sech}^2(\eta_n)]$ are also used, where $\boldsymbol{\eta} = [\eta_1, \eta_2, \ldots, \eta_n]^T \in \Re^n$, diag[$\bullet$] denotes a diagonal matrix, $\tanh(\bullet)$ and $\mathrm{sech}^2(\bullet) = 1/\cosh^2(\bullet)$ represent the hyperbolic tangent function and its derivative, respectively. In addition, $\Re^+$ denotes a set of positive real numbers.

2.2. Kinematic and dynamic models

Consider a class of underactuated AUV whose 5-DOF kinematic and dynamic models are described as follows:[21,22]

$$\dot{\boldsymbol{\eta}} = \begin{bmatrix} \dot{\boldsymbol{\eta}}_1 \\ \dot{\boldsymbol{\eta}}_2 \end{bmatrix} = \underbrace{\begin{bmatrix} \boldsymbol{T}_1(\boldsymbol{\eta}_2) & 0 \\ 0 & \boldsymbol{T}_2(\boldsymbol{\eta}_2) \end{bmatrix}}_{\boldsymbol{T}(\boldsymbol{\eta}_2)} \underbrace{\begin{bmatrix} \boldsymbol{v}_1 \\ \boldsymbol{v}_2 \end{bmatrix}}_{\boldsymbol{v}}, \tag{1}$$

where $\boldsymbol{T}_1(\boldsymbol{\eta}_2)$ and $\boldsymbol{T}_2(\boldsymbol{\eta}_2)$ are given by

$$\boldsymbol{T}_1(\boldsymbol{\eta}_2) = \begin{bmatrix} \cos(\psi)\cos(\theta) & -\sin(\psi) & \sin(\theta)\cos(\psi) \\ \sin(\psi)\cos(\theta) & \cos(\psi) & \sin(\theta)\sin(\psi) \\ -\sin(\theta) & 0 & \cos(\theta) \end{bmatrix}, \quad \boldsymbol{T}_2(\boldsymbol{\eta}_2) = \begin{bmatrix} 1 & 0 \\ 0 & 1/\cos(\theta) \end{bmatrix},$$

and

$$\begin{aligned}
\dot{u} &= \frac{m_{22}}{m_{11}} vr - \frac{m_{33}}{m_{11}} wq - \frac{d_{11}}{m_{11}} u + \frac{1}{m_{11}} \tau_u - \frac{1}{m_{11}} \tau_{wu}(t), \\
\dot{v} &= -\frac{m_{11}}{m_{22}} ur - \frac{d_{22}}{m_{22}} v - \frac{1}{m_{22}} \tau_{wv}(t), \\
\dot{w} &= \frac{m_{11}}{m_{33}} uq - \frac{d_{33}}{m_{33}} w - \frac{1}{m_{33}} \tau_{ww}(t), \\
\dot{q} &= \frac{m_{33} - m_{11}}{m_{55}} uw - \frac{d_{55}}{m_{55}} q - \frac{\rho g \nabla G M_L \sin(\theta)}{m_{55}} + \frac{1}{m_{55}} \tau_q - \frac{1}{m_{55}} \tau_{wq}(t), \\
\dot{r} &= \frac{m_{11} - m_{22}}{m_{66}} uv - \frac{d_{66}}{m_{66}} r + \frac{1}{m_{66}} \tau_r - \frac{1}{m_{66}} \tau_{wr}(t),
\end{aligned} \tag{2}$$

where x, y, z, θ and ψ denote the positions (i.e. the surge, sway and heave displacements), and orientations (i.e. pitch and yaw angles), respectively, in the earth-fixed frame, which are denoted by the vector $\boldsymbol{\eta} = [\boldsymbol{\eta}_1^T, \boldsymbol{\eta}_2^T]^T$, where $\boldsymbol{\eta}_1 = [x, y, z]^T$ and $\boldsymbol{\eta}_2 = [\theta, \psi]^T$. The signals u, v, w, q and r represent the surge, sway, heave, pitch and yaw velocities in the body-fixed frame which are denoted by the vector $\boldsymbol{v} = [\boldsymbol{v}_1^T, \boldsymbol{v}_2^T]^T$, where $\boldsymbol{v}_1 = [u, v, w]^T$ and $\boldsymbol{v}_2 = [q, r]^T$. The control inputs τ_u, τ_q and τ_r are provided by the actuators with the limited torque which are simply modeled as follows in this

https://doi.org/10.1017/S0263574717000455 Published online by Cambridge University Press

paper:

$$\tau_k = \begin{cases} \tau_{k,\max}, & \text{if } \tau_k > \tau_{k,\max} \\ \tau_k, & \text{if } \tau_{k,\min} \le \tau_k \le \tau_{k,\max}, \\ \tau_{k,\min}, & \text{if } \tau_k < \tau_{k,\min} \end{cases} \quad k = u, q, r \tag{3}$$

where $\tau_{k,\max} > 0$ and $\tau_{k,\min} < 0$ denote the upper and lower limits of the actuator saturation nonlinearity, respectively. The signals $\tau_{wu}(t)$, $\tau_{wv}(t)$, $\tau_{ww}(t)$, $\tau_{wq}(t)$, $\tau_{wr}(t) \in \Re$ are bounded time-varying disturbances and unmodeled dynamics, $m_{11} = m - X_{\dot{u}}$, $m_{22} = m - Y_{\dot{v}}$, $m_{33} = m - Z_{\dot{w}}$, $m_{55} = I_y - M_{\dot{q}}$ $m_{66} = I_z - N_{\dot{r}}$, $d_{11} = -X_u$, $d_{22} = -Y_v$, $d_{33} = -Z_w$, $d_{55} = -M_q$ and $d_{66} = -N_r$ where m denotes the mass of the vehicle, I_y and I_z are the moments of the inertia about the pitch and yaw rotation axes, and other symbols represent hydrodynamic derivatives.[23] In addition, ρ, g, ∇ and GM_L represent the water density, gravity acceleration, displaced volume of the water, and longitudinal metacentric height, respectively, according to ref. [21]. It should be noted that the above models are valid when AUVs are operating at low speeds and they are equipped with independent internal or external roll actuators. The interested readers are referred to ref. [21] for more details and discussions.

To develop the controller in the next section, the kinematic model of (1) is expressed in the actuated degrees of freedom as follows:

$$\dot{\boldsymbol{\eta}} = \boldsymbol{S}(\boldsymbol{\eta})\boldsymbol{\upsilon} + \boldsymbol{\delta}(\boldsymbol{\eta}, \boldsymbol{w}), \tag{4}$$

where $\boldsymbol{S}(\boldsymbol{\eta})$ denotes a new kinematic matrix, $\boldsymbol{\upsilon} = [u,\ q,\ r]^T$ and $\boldsymbol{w} = [v, w]^T$ are considered as new velocity vectors in the actuated and unactuated directions, respectively, and $\boldsymbol{\delta}(\boldsymbol{\eta}, \boldsymbol{w}) \in \Re^5$ denotes a vector of the kinematic disturbances which is defined as follows:

$$\boldsymbol{S}(\boldsymbol{\eta}) = \begin{bmatrix} \cos(\psi)\cos(\theta) & 0 & 0 \\ \sin(\psi)\cos(\theta) & 0 & 0 \\ -\sin(\theta) & 0 & 0 \\ 0 & 1 & 0 \\ 0 & 0 & 1/\cos(\theta) \end{bmatrix}, \quad \boldsymbol{\delta}(\boldsymbol{\eta}, \boldsymbol{w}) = \begin{bmatrix} -v\sin(\psi) + w\sin(\theta)\cos(\psi) \\ v\cos(\psi) + w\sin(\theta)\sin(\psi) \\ w\cos(\theta) \\ 0 \\ 0 \end{bmatrix}. \tag{5}$$

The actuated dynamics of the AUV, i.e. the surge, pitch and yaw dynamics are stated in the following form:

$$\boldsymbol{M}_1\dot{\boldsymbol{\upsilon}}(t) + \boldsymbol{C}_1(\boldsymbol{w})\boldsymbol{\upsilon}(t) + \boldsymbol{D}_1\boldsymbol{\upsilon}(t) + \boldsymbol{G}_1(\boldsymbol{\eta}) + \boldsymbol{\tau}_{w1}(t) = \boldsymbol{\tau}_a(t), \tag{6}$$

where $\boldsymbol{\tau}_a = [\tau_u,\ \tau_q,\ \tau_r]^T$ denotes a vector of the control inputs, $\boldsymbol{M}_1 \in \Re^{3\times3}$ denotes the inertia matrix, $\boldsymbol{C}_1(\boldsymbol{w}) \in \Re^{3\times3}$ shows the centripetal and Coriolis forces, $\boldsymbol{D}_1 \in \Re^{3\times3}$ denotes the hydrodynamic damping matrix, $\boldsymbol{G}_1(\boldsymbol{\eta}) \in \Re^3$ is a vector of the gravity forces, $\boldsymbol{\tau}_{w1}(t) \in \Re^3$ denotes the unmodeled dynamics, constant and time-varying disturbances induced by waves and ocean currents, which are defined as follows:

$$\boldsymbol{M}_1 = \begin{bmatrix} m_{11} & 0 & 0 \\ 0 & m_{55} & 0 \\ 0 & 0 & m_{66} \end{bmatrix}, \quad \boldsymbol{C}_1(\boldsymbol{w}) = \begin{bmatrix} 0 & m_{33}w & -m_{22}v \\ (m_{11} - m_{33})w & 0 & 0 \\ (m_{22} - m_{11})v & 0 & 0 \end{bmatrix},$$

$$\boldsymbol{D}_1 = \begin{bmatrix} d_{11} & 0 & 0 \\ 0 & d_{55} & 0 \\ 0 & 0 & d_{66} \end{bmatrix}, \quad \boldsymbol{G}_1(\boldsymbol{\eta}) = \begin{bmatrix} 0 \\ \rho g \nabla G M_L \sin(\theta) \\ 0 \end{bmatrix}, \quad \boldsymbol{\tau}_{w1}(t) = \begin{bmatrix} \tau_{wu}(t) \\ \tau_{wq}(t) \\ \tau_{wr}(t) \end{bmatrix},$$

The unactuated dynamics of AUV, i.e. the sway and heave dynamics are written as follows:

$$\bar{\boldsymbol{M}}_1\dot{\boldsymbol{w}} + \bar{\boldsymbol{C}}_1(\boldsymbol{\upsilon})\boldsymbol{\upsilon} + \bar{\boldsymbol{D}}w + \bar{\boldsymbol{\tau}}_{w1}(t) = \boldsymbol{0} \tag{7}$$

https://doi.org/10.1017/S0263574717000455 Published online by Cambridge University Press

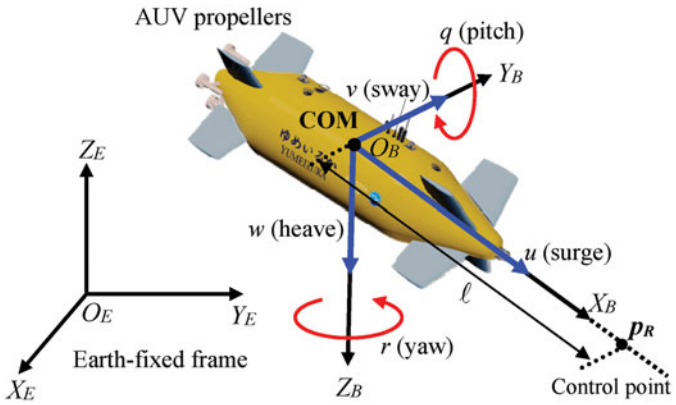

Fig. 1. Three-dimensional configuration of an underactuated autonomous underwater vehicle. Photo courtesy of http://auvac.org/platforms/view/234.

where

$$\bar{\boldsymbol{M}}_1 = \begin{bmatrix} m_{22} & 0 \\ 0 & m_{33} \end{bmatrix}, \ \bar{\boldsymbol{C}}_1(\upsilon) = \begin{bmatrix} 0 & 0 & m_{11}u \\ 0 & -m_{11}u & 0 \end{bmatrix}, \ \bar{\boldsymbol{D}}_1(\boldsymbol{\eta}) = \begin{bmatrix} d_{22} & 0 \\ 0 & d_{33} \end{bmatrix}, \ \bar{\boldsymbol{\tau}}_{w1}(t) = \begin{bmatrix} \tau_{wv}(t) \\ \tau_{ww}(t) \end{bmatrix}. \tag{8}$$

Assumption 1. The sway and heave velocities of the vehicle are passive-bounded in the sense that $\sup_{t\geq 0} \|\boldsymbol{w}(t)\| < B_w$.

Reamrk 1. As frequently reported in the literature,[19,22,24,25] it is easy to systematically analyze the passive-boundedness property of the sway and heave velocities of the ocean vehicles. Since the hydrodynamic damping forces in (7) are dominant in the sway and heave directions in practice and, as a result, the sway and heave velocities are damped out by such forces, the above assumption is reasonably accepted. The interested readers are referred to refs. [22] and [25] for further discussions about Assumption 1.

Reamrk 2. In practice, the response of the actuators and thrusters is much faster than the vehicle response. Consequently, their dynamics are reasonably ignored in this paper and their slight effects are considered as unmodeled dynamics which are included in the term $\boldsymbol{\tau}_{w1}(t)$ in (6).

Assumption 2. The disturbance vectors $\boldsymbol{\tau}_{w1}(t) \in \Re^3$ and $\bar{\boldsymbol{\tau}}_{w1}(t) \in \Re^2$ are bounded in the sense that $\|\boldsymbol{\tau}_{w1}(t)\| \leq \lambda_{w11}$ and $\|\bar{\boldsymbol{\tau}}_{w1}(t)\| \leq \bar{\lambda}_{w11}$ where λ_{w11} and $\bar{\lambda}_{w11}$ show the positive constants.

Property 1. The following properties are valid for the dynamic model (6):

P1.1: $\boldsymbol{M}_1$ is a positive-definite and symmetric matrix which is upper and lower bounded such that $\lambda_{m_1}\|\boldsymbol{x}\|^2 \leq \boldsymbol{x}^T\boldsymbol{M}_1\boldsymbol{x} \leq \lambda_{M_1}\|\boldsymbol{x}\|^2 \ \forall \boldsymbol{x} \in \Re^3$, and $0 < \lambda_{m_1} \leq \lambda_{M_1} < \infty$ where $\lambda_{m_1} := \lambda_{\min}(\boldsymbol{M}_1)$ and $\lambda_{M_1} := \lambda_{\max}(\boldsymbol{M}_1)$.

P1.2: Considering Assumption 1, the following upper bounds are valid for the presented model: $\|\boldsymbol{C}_1(\boldsymbol{w})\| \leq \lambda_{C_1}\|\boldsymbol{w}\| \leq \lambda_{C_{1w}}$, $\|\boldsymbol{D}_1\| \leq \lambda_{D_1}$, $\|\boldsymbol{G}_1(\boldsymbol{\eta}))\| \leq \lambda_{G_1}$, $\forall \boldsymbol{\eta} \in \Re^5$, $\boldsymbol{w} \in \Re^2$ where λ_{C_1}, $\lambda_{C_{1w}}$, λ_{D_1} and λ_{G_1} are some positive scalar constants.

2.3. Coordinate transformation

Since the 3D position tracking control of underactuated AUVs is of interest in this paper, the position coordinates in x, y and z directions should be chosen in the earth-fixed frame. One simple choice is the position of the center of mass (COM) as illustrated in Fig. 1. However, the main problems of this choice are that (i) the controller will not sense any disturbance in the pitch and yaw directions based on the presented AUV model (1) and (2); (ii) the COM position will not be affected by the yaw and pitch control inputs. Therefore, the following coordinate transformation is introduced which includes

https://doi.org/10.1017/S0263574717000455 Published online by Cambridge University Press

all DOFs to incorporate the AUV dynamics in all directions and to involve all control inputs:

$$\begin{aligned} \boldsymbol{y} = \boldsymbol{h}(\boldsymbol{\eta}) = \boldsymbol{p}_R^E = \boldsymbol{O}_B^E + \boldsymbol{T}_1(\boldsymbol{\eta}_2)\boldsymbol{p}_R^B \\ = [x + \ell\cos(\theta)\cos(\psi),\ \ y + \ell\cos(\theta)\sin(\psi),\ \ z - \ell\sin(\theta)]^T, \end{aligned} \tag{9}$$

where $\boldsymbol{O}_B^E$ represents the coordinates of O_B in the earth-fixed frame $\{O_E X_E Y_E Z_E\}$ in Fig. 1, $\boldsymbol{p}_R^B = [\ell, 0, 0]^T$ denotes the coordinates of a virtual reference point in the body-fixed frame $\{O_B X_B Y_B Z_B\}$ which is called the control point in this paper, $\boldsymbol{p}_R^E$ denotes the coordinates of the virtual control point $P_R$in the earth-fixed frame which is represented by $\boldsymbol{y}$ for the notation simplicity, and ℓ is a constant positive parameter. By differentiating (9) and substituting (4), one gets

$$\dot{\boldsymbol{y}} = \boldsymbol{J}(\boldsymbol{\eta})\boldsymbol{\upsilon} + \boldsymbol{J}_\delta(\boldsymbol{\eta}, \boldsymbol{w}), \tag{10}$$

where

$$\boldsymbol{J}(\boldsymbol{\eta}) = \boldsymbol{J}_h(\boldsymbol{\eta})\boldsymbol{S}(\boldsymbol{\eta}) = \begin{bmatrix} \cos(\psi)\cos(\theta) & -\ell\sin(\theta)\cos(\psi) & -\ell\sin(\psi) \\ \sin(\psi)\cos(\theta) & -\ell\sin(\theta)\sin(\psi) & \ell\cos(\psi) \\ -\sin(\theta) & -\ell\cos(\theta) & 0 \end{bmatrix}, \tag{11}$$

$$\boldsymbol{J}_\delta(\boldsymbol{\eta}, \boldsymbol{w}) = \boldsymbol{J}_h(\boldsymbol{\eta})\boldsymbol{\delta}(\boldsymbol{\eta}, \boldsymbol{w}) = \begin{bmatrix} -v\sin(\psi) + w\sin(\theta)\cos(\psi) \\ v\cos(\psi) + w\sin(\theta)\sin(\psi) \\ w\cos(\theta) \end{bmatrix}, \tag{12}$$

where $\boldsymbol{J}_h(\boldsymbol{\eta}) := \partial\boldsymbol{h}(\boldsymbol{\eta})/\partial\boldsymbol{\eta}$ denotes the Jacobian Matrix. In contrast to the kinematic matrix $\boldsymbol{S}(\boldsymbol{\eta})$, there is no singularity in the matrix $\boldsymbol{J}(\boldsymbol{\eta})$ for all $\theta,\ \psi \in \Re$. Then, one may write

$$\boldsymbol{\upsilon} = \boldsymbol{J}^{-1}(\boldsymbol{\eta})(\dot{\boldsymbol{y}} - \boldsymbol{J}_\delta(\boldsymbol{\eta}, \boldsymbol{w})), \tag{13}$$

Once again, the time-derivative of (10) yields $\ddot{\boldsymbol{y}} = \dot{\boldsymbol{J}}\upsilon + \boldsymbol{J}\dot{\upsilon} + \dot{\boldsymbol{J}}_\delta$ which is re-written as $\dot{\boldsymbol{\upsilon}} = \boldsymbol{J}^{-1}\ddot{\boldsymbol{y}} - \boldsymbol{J}^{-1}\dot{\boldsymbol{J}}\upsilon - \boldsymbol{J}^{-1}\dot{\boldsymbol{J}}_\delta$ which together with (13) and (6) yield

$$\begin{aligned} \boldsymbol{M}_1\boldsymbol{J}^{-1}\ddot{\boldsymbol{y}} - \boldsymbol{M}_1\boldsymbol{J}^{-1}\dot{\boldsymbol{J}}(\boldsymbol{J}^{-1}\dot{\boldsymbol{y}} - \boldsymbol{J}^{-1}\boldsymbol{J}_\delta) - \boldsymbol{M}_1\boldsymbol{J}^{-1}\dot{\boldsymbol{J}}_\delta + \boldsymbol{C}_1\boldsymbol{J}^{-1}\dot{\boldsymbol{y}} \\ - \boldsymbol{C}_1\boldsymbol{J}^{-1}\boldsymbol{J}_\delta + \boldsymbol{D}_1\boldsymbol{J}^{-1}\dot{\boldsymbol{y}} - \boldsymbol{D}_1\boldsymbol{J}^{-1}\boldsymbol{J}_\delta + \boldsymbol{G}_1 + \boldsymbol{\tau}_{w1} = \boldsymbol{\tau}_a. \end{aligned} \tag{14}$$

Then, by taking the following equalities into account from (4), (7) and (13)

$$\boldsymbol{M}_1\boldsymbol{J}^{-1}\dot{\boldsymbol{J}}\boldsymbol{J}^{-1}\boldsymbol{J}_\delta - \boldsymbol{M}_1\boldsymbol{J}^{-1}\dot{\boldsymbol{J}}_\delta = -\boldsymbol{M}_1 d(\boldsymbol{J}^{-1}\boldsymbol{J}_\delta)/dt,$$

$$\begin{aligned} \frac{d}{dt}(\boldsymbol{J}^{-1}\boldsymbol{J}_\delta) = \frac{\partial(\boldsymbol{J}^{-1}\boldsymbol{J}_\delta)}{\partial\boldsymbol{\eta}}\boldsymbol{S}\boldsymbol{J}^{-1}\dot{\boldsymbol{y}} - \frac{\partial(\boldsymbol{J}^{-1}\boldsymbol{J}_\delta)}{\partial\boldsymbol{w}}\bar{\boldsymbol{M}}_1^{-1}\bar{\boldsymbol{D}}w - \frac{\partial(\boldsymbol{J}^{-1}\boldsymbol{J}_\delta)}{\partial\boldsymbol{w}}\bar{\boldsymbol{M}}_1^{-1}\bar{\boldsymbol{\tau}}_{w1} \\ - \frac{\partial(\boldsymbol{J}^{-1}\boldsymbol{J}_\delta)}{\partial\boldsymbol{w}}\bar{\boldsymbol{M}}_1^{-1}\bar{\boldsymbol{C}}_1(\boldsymbol{J}^{-1}\dot{\boldsymbol{y}})\boldsymbol{J}^{-1}\dot{\boldsymbol{y}} + 2\frac{\partial(\boldsymbol{J}^{-1}\boldsymbol{J}_\delta)}{\partial\boldsymbol{w}}\bar{\boldsymbol{M}}_1^{-1}\bar{\boldsymbol{C}}_1(\boldsymbol{J}^{-1}\boldsymbol{J}_\delta)\boldsymbol{J}^{-1}\dot{\boldsymbol{y}} \\ - \frac{\partial(\boldsymbol{J}^{-1}\boldsymbol{J}_\delta)}{\partial\boldsymbol{w}}\bar{\boldsymbol{M}}_1^{-1}\bar{\boldsymbol{C}}_1(\boldsymbol{J}^{-1}\boldsymbol{J}_\delta)\boldsymbol{J}^{-1}\boldsymbol{J}_\delta, \end{aligned}$$

and considering the force-torque transformation $\boldsymbol{\tau}_a = \boldsymbol{J}^T(\boldsymbol{\eta})\boldsymbol{F}_{p_R}$ from the virtual work theory,[26] where $\boldsymbol{F}_{p_R} \in \Re^3$ is the force acting on the virtual control point P_R in Fig. 1, and multiplying both sides of (14) by $\boldsymbol{J}^{-T}(\boldsymbol{\eta})$, it is straightforward to obtain the following earth-fixed frame representation:

$$\boldsymbol{M}_2(\boldsymbol{\eta})\ddot{\boldsymbol{y}} + \boldsymbol{C}_2(\boldsymbol{\eta},\ \dot{\boldsymbol{y}})\dot{\boldsymbol{y}} + \boldsymbol{D}_2(\boldsymbol{\eta})\dot{\boldsymbol{y}} + \boldsymbol{d}(\boldsymbol{\eta}, \boldsymbol{w},\ \dot{\boldsymbol{y}}) + \boldsymbol{G}_2(\boldsymbol{\eta}) + \boldsymbol{\tau}_{w2}(\boldsymbol{\eta}, \boldsymbol{w}, t) = \boldsymbol{F}_{p_R} = \boldsymbol{J}^{-T}(\boldsymbol{\eta})\boldsymbol{\tau}_a, \tag{15}$$

where $\boldsymbol{M}_2(\boldsymbol{\eta}),\ \boldsymbol{C}_2(\boldsymbol{\eta},\ \dot{\boldsymbol{y}}),\ \boldsymbol{D}_2(\boldsymbol{\eta}),\ \boldsymbol{d}(\boldsymbol{\eta}, \boldsymbol{w},\ \dot{\boldsymbol{y}}),\ \boldsymbol{G}_2(\boldsymbol{\eta})$ and $\boldsymbol{\tau}_{w2}(\boldsymbol{\eta}, \boldsymbol{w}, t)$ are derived as follows:

$$\boldsymbol{M}_2(\boldsymbol{\eta}) = \boldsymbol{J}^{-T}(\boldsymbol{\eta})\boldsymbol{M}_1\boldsymbol{J}^{-1}(\boldsymbol{\eta}),$$

https://doi.org/10.1017/S0263574717000455 Published online by Cambridge University Press

$$\boldsymbol{C}_2(\boldsymbol{\eta},\ \dot{\boldsymbol{y}}) = -\boldsymbol{J}^{-T}(\boldsymbol{\eta})\boldsymbol{M}_1\boldsymbol{J}^{-1}\dot{\boldsymbol{J}}\boldsymbol{J}^{-1}(\boldsymbol{\eta}),$$

$$\boldsymbol{D}_2(\boldsymbol{\eta}) = \boldsymbol{J}^{-T}(\boldsymbol{\eta})\boldsymbol{D}_1\boldsymbol{J}^{-1}(\boldsymbol{\eta}),$$

$$\begin{aligned}\boldsymbol{d}(\boldsymbol{\eta},\boldsymbol{w},\ \dot{\boldsymbol{y}}) = \boldsymbol{J}^{-T}(\boldsymbol{\eta})(\boldsymbol{C}_1 - \boldsymbol{M}_1\frac{\partial(\boldsymbol{J}^{-1}\boldsymbol{J}_\delta)}{\partial\boldsymbol{\eta}}\boldsymbol{S} - 2\boldsymbol{M}_1\frac{\partial(\boldsymbol{J}^{-1}\boldsymbol{J}_\delta)}{\partial\boldsymbol{w}}\bar{\boldsymbol{M}}_1^{-1}\bar{\boldsymbol{C}}_1(\boldsymbol{J}^{-1}\boldsymbol{J}_\delta))\boldsymbol{J}^{-1}(\boldsymbol{\eta})\dot{\boldsymbol{y}}\\ + \boldsymbol{J}^{-T}(\boldsymbol{\eta})\boldsymbol{M}_1\frac{\partial(\boldsymbol{J}^{-1}\boldsymbol{J}_\delta)}{\partial\boldsymbol{w}}\bar{\boldsymbol{M}}_1^{-1}\bar{\boldsymbol{C}}_1(\boldsymbol{J}^{-1}\dot{\boldsymbol{y}})\boldsymbol{J}^{-1}(\boldsymbol{\eta})\dot{\boldsymbol{y}},\end{aligned}$$

$$\boldsymbol{G}_2(\boldsymbol{\eta}) = \boldsymbol{J}^{-T}(\boldsymbol{\eta})\boldsymbol{G}_1,$$

and

$$\begin{aligned}\boldsymbol{\tau}_{w2}(\boldsymbol{\eta},\boldsymbol{w},t) = \boldsymbol{J}^{-T}(\boldsymbol{\eta})(-\boldsymbol{C}_1\boldsymbol{J}^{-1}\boldsymbol{J}_\delta - \boldsymbol{D}_1\boldsymbol{J}^{-1}\boldsymbol{J}_\delta + \boldsymbol{\tau}_{w1} + \boldsymbol{M}_1\frac{\partial(\boldsymbol{J}^{-1}\boldsymbol{J}_\delta)}{\partial\boldsymbol{w}}\bar{\boldsymbol{M}}_1^{-1}\bar{\boldsymbol{D}}w\\ + \boldsymbol{M}_1\frac{\partial(\boldsymbol{J}^{-1}\boldsymbol{J}_\delta)}{\partial\boldsymbol{w}}\bar{\boldsymbol{M}}_1^{-1}\bar{\boldsymbol{\tau}}_{w1} + \boldsymbol{M}_1\frac{\partial(\boldsymbol{J}^{-1}\boldsymbol{J}_\delta)}{\partial\boldsymbol{w}}\bar{\boldsymbol{M}}_1^{-1}\bar{\boldsymbol{C}}_1(\boldsymbol{J}^{-1}\boldsymbol{J}_\delta)\boldsymbol{J}^{-1}\boldsymbol{J}_\delta).\end{aligned}$$

These matrices are not required for the controller design in the next section. By considering that $\boldsymbol{J}(\boldsymbol{\eta}) \in \Re^{3\times3}$ is a full rank matrix, and recalling Property 1, and referring to ref. [26], it is easy to prove that the model of (15) satisfies the following properties:

Property 2. The following properties hold for the proposed model (15):

P2.1: $\boldsymbol{M}_2(\boldsymbol{\eta})$ is a symmetric and positive-definite matrix which is lower and upper bounded as $\lambda_{m_2}\|\boldsymbol{x}\|^2 \le \boldsymbol{x}^T\boldsymbol{M}_2(\boldsymbol{\eta})\boldsymbol{x} \le \lambda_{M_2}\|\boldsymbol{x}\|^2\ \forall\boldsymbol{x}\in\Re^3, \boldsymbol{\eta}\in\Re^5$, and $0 < \lambda_{m_2} \le \lambda_{M_2} < \infty$ where $\lambda_{m_2} := \min_{\forall\eta\in\Re^5}\lambda_{\min}(\boldsymbol{M}_2(\boldsymbol{\eta}))$ and $\lambda_{M_2} := \max_{\forall\eta\in\Re^5}\lambda_{\max}(\boldsymbol{M}_2(\boldsymbol{\eta}))$.

P2.2: The matrix $\dot{\boldsymbol{M}}_2(\boldsymbol{\eta}) - 2\boldsymbol{C}_2(\boldsymbol{\eta},\ \dot{\boldsymbol{y}})$ is skew-symmetric, that is, $\boldsymbol{x}^T(\dot{\boldsymbol{M}}_2(\boldsymbol{\eta}) - 2\boldsymbol{C}_2(\boldsymbol{\eta},\ \dot{\boldsymbol{y}}))\boldsymbol{x} = 0,\ \ \forall\boldsymbol{x}, \dot{\boldsymbol{y}}\in\Re^3$.

P2.3: The centripetal-Coriolis matrix satisfies the following relationship:

$$\boldsymbol{C}_2(\boldsymbol{\eta},\ \boldsymbol{x}_1)\boldsymbol{x}_2 = \boldsymbol{C}_2(\boldsymbol{\eta},\ \boldsymbol{x}_2)\boldsymbol{x}_1\ \ \forall\boldsymbol{x}_1,\boldsymbol{x}_2\in\Re^3$$

P2.4: Based on P1.2 and Assumptions 1 and 2, there exist positive scalar constants $\lambda_{C_2}, \lambda_{G_2}$ and λ_{w2} such that $\|\boldsymbol{C}_2(\boldsymbol{\eta},\ \dot{\boldsymbol{y}})\| \le \lambda_{C_2}\|\dot{\boldsymbol{y}}\|,\ \ \|\boldsymbol{G}_2(\boldsymbol{\eta})\| \le \lambda_{G_2}$ and $\|\boldsymbol{\tau}_{w2}(\boldsymbol{\eta},\boldsymbol{w},t)\| \le \lambda_{w2}$.

P2.5: The damping term $\boldsymbol{d}(\boldsymbol{\eta},\boldsymbol{w},\ \dot{\boldsymbol{y}})$ satisfies the following Lipschitz condition:

$$\|\boldsymbol{d}(\boldsymbol{\eta},\boldsymbol{w},\ \boldsymbol{x}_1) - \boldsymbol{d}(\boldsymbol{\eta},\boldsymbol{w},\ \boldsymbol{x}_2)\| \le d_{M1}\|\boldsymbol{x}_1 - \boldsymbol{x}_2\| + d_{M2}\|\boldsymbol{x}_1 - \boldsymbol{x}_2\|^2\ \ \forall\boldsymbol{x}_1,\boldsymbol{x}_2\in\Re^3$$

where d_{M1} and d_{M2} are the unknown positive scalar constants.

P2.6: The matrix $\boldsymbol{D}_2(\boldsymbol{\eta})$ satisfies the following inequality

$$\lambda_{d_2}\|\boldsymbol{x}\|^2 \le \boldsymbol{x}^T\boldsymbol{D}_2(\boldsymbol{\eta})\boldsymbol{x} \le \lambda_{D_2}\|\boldsymbol{x}\|^2\ \forall\boldsymbol{x}\in\Re^3,\ \boldsymbol{\eta}\in\Re^5$$

where $0 < \lambda_{d_2} \le \lambda_{D_2} < \infty$ and $\lambda_{d_2} := \min_{\forall\eta\in\Re^5}\lambda_{\min}(\boldsymbol{D}_2(\boldsymbol{\eta}))$ and $\lambda_{D_2} := \max_{\forall\eta\in\Re^5}\lambda_{\max}(\boldsymbol{D}_2(\boldsymbol{\eta}))$.

https://doi.org/10.1017/S0263574717000455 Published online by Cambridge University Press

2.4. Control objectives

The following tracking problem is addressed in this paper by considering Assumptions 1 and 2:

Definition 1. Given a smooth bounded desired trajectory $\boldsymbol{y}_d(t) : [0, \infty) \to \Re^3$ which is generated by an open-loop motion planner whose motion equations are given by (1) and (2), the *control objective*, which is discussed in this paper, is to design an OFB tracking control law for an underactuated AUV system (1) and (2) such that it forces the tracking errors, $\boldsymbol{e}(t) := \boldsymbol{y}(t) - \boldsymbol{y}_d(t) \in \Re^3$, to converge to small balls containing the origin under following conditions:

C1. The vehicle parameters are unknown, and the vehicle is subjected to constant or time-varying disturbances induced by the waves and ocean currents;

C2. The velocity measurements are not available for the feedback;

C3. The AUV actuators are saturated in the sense that $|\tau_u| < \tau_{u\max}$, $|\tau_q| < \tau_{q\max}$ and $|\tau_r| < \tau_{r\max}$.

The following assumptions are also essential to meet the above control objectives:

Assumption 3. The measurements of the output vector $\boldsymbol{y} \in \Re^3$ are available in real-time. For this purpose, it is assumed that the position and heading sensors are used to obtain the output measurements in (9).

Assumption 4. The desired trajectory $\boldsymbol{y}_d(t)$ is chosen such that $\boldsymbol{y}_d(t)$, $\dot{\boldsymbol{y}}_d(t)$ and $\ddot{\boldsymbol{y}}_d(t)$ are all bounded signals such that $\sup_{t\geq 0} \|\boldsymbol{y}_d(t)\| < B_{dp}$, $\sup_{t\geq 0} \|\dot{\boldsymbol{y}}_d(t)\| < B_{dv}$ and $\sup_{t\geq 0} \|\ddot{\boldsymbol{y}}_d(t)\| < B_{da}$ where B_{dp}, B_{dv} and B_{da} are some bounded positive constants.

Definition 2. Given a positive constant M_i, a function $s_i : \Re \to \Re : \xi \to s_i(\xi)$ is said to be a saturation function with bound M_i, if it is locally Lipschitz, non-decreasing, and satisfies: (i) $\xi s_i(\xi) > 0$, $\forall \xi \neq 0$; and (ii) $|s_i(\xi)| \leq M_i$, $\forall \xi \in \Re$.

The common examples of such functions are $s_i(\xi) = \tanh(\xi)$ and $s_i(\xi) = \xi/\sqrt{1+\xi^2}$ with $M_i = 1$. A strictly increasing continuously differentiable function satisfying the above definition has the following properties.

Lemma 1. Let $s_i : \Re \to \Re : \xi \to s_i(\xi)$ be a strictly increasing continuously differentiable saturation function including the hyperbolic tangent function with bound M_i, let k_1 and k_2 be the positive constants, and $s_i' : \xi \to ds_i/d\xi$ where $0 < s_i'(\xi) \leq s_{iM}'$, $\forall \xi \in \Re$. Then, the following properties can be proved:

(i) $s_i^2(k_1\xi)/(2k_1 s_{iM}') \leq \int_0^\xi s_i(k_1 r)dr \leq k_1 s_{iM}' \xi^2/2$, $\forall \xi \in \Re$, which results in the inequality $\tanh^2(k_1\xi)/(2k_1) \leq \ln(\cosh(\xi)) \leq k_1\xi^2/2$, $\forall \xi \in \Re$;

(ii) $\int_0^\xi s_i(kr)dr > 0$, $\forall \xi \neq 0$, $\int_0^\xi s_i(kr)dr \to \infty$ as $|\xi| \to \infty$, $\ln(\cosh(\xi)) > 0$, $\forall \xi \neq 0$ and $\ln(\cosh(\xi)) \to \infty$ as $|\xi| \to \infty$;

(iii) $|s_i(k_1x + k_2y) - s_i(k_2y)| \leq s_{iM}' k_1|x|$, $\forall x, y \in \Re$ and $|s_i(x) - s_i(x-y)| \leq s_{iM}'|y|$, $\forall x, y \in \Re$, $|\tanh(k_1x + k_2y) - \tanh(k_2y)| \leq k_1|x|$, $\forall x, y \in \Re$, $|\tanh(x) - \tanh(x-y)| \leq |y|$, $\forall x, y \in \Re$;

(iv) $|s_i(k_1x)| \leq s_{iM}' k_1|x|$, $\forall x \in \Re$ and $|\tanh(k_1x)| \leq k_1|x|$, $\forall x \in \Re$;

(v) From item (iv), it follows that $|s_i(x)|^2 \leq s_{iM}'|x||s_i(x)| = s_{iM}' x\, s_i(x)$, $\forall x \in \Re$, and as a result, one gets $|\tanh(x)|^2 \leq |x||\tanh(x)| = x\tanh(x)$, $\forall x \in \Re$ and $\boldsymbol{x}^T \boldsymbol{\Psi}\, \boldsymbol{Tanh}(\boldsymbol{x}) \geq \lambda_{\min}\{\boldsymbol{\Psi}\}\|\boldsymbol{Tanh}(\boldsymbol{x})\|^2$, $\forall \boldsymbol{x} \in \Re^n$, $\boldsymbol{\Psi} \in \Re^{n\times n}$;

(vi) From item (i), it follows that $s_i^2(\xi) \leq s_{iM}'^2 \xi^2$, $\forall \xi \in \Re$ and $\tanh^2(\xi) \leq \xi^2$, $\forall \xi \in \Re$ which leads to $\|\boldsymbol{Tanh}(\boldsymbol{x})\|^2 \leq \|\boldsymbol{x}\|^2$.

Proof. See ref. [27].

Lemma 2 [28]**.** The inequality $h\|\boldsymbol{x}\| - \boldsymbol{x}^{\mathrm{T}} h\, \boldsymbol{Tanh}(\nu h\, \boldsymbol{x}/\varepsilon_t) \leq n\varepsilon_t$ holds for any $\varepsilon_t > 0$, and for any $\forall \boldsymbol{x} \in \Re^n$ and $h \in \Re$ where $\boldsymbol{Tanh}(\nu h\, \boldsymbol{x}/\varepsilon_t) := [\tanh(\nu h\, x_1/\varepsilon_t), \ldots, \tanh(\nu h\, x_n/\varepsilon_t)]^T$ and ν is a constant which satisfies $\nu = e^{-(\nu+1)}$, i.e. $\nu = 0.2785$.

https://doi.org/10.1017/S0263574717000455 Published online by Cambridge University Press

3. Saturated Output Feedback Tracking Controller

3.1. Controller design

In this section, a saturated OFB controller is designed by using the hyperbolic tangent function, which is a simple case of the saturation functions, to satisfy the control objectives which were defined in Definition 1. For this purpose, the tracking and state estimation error vectors are defined as $\boldsymbol{e}(t) := \boldsymbol{y}(t) - \boldsymbol{y}_d(t)$ and $\boldsymbol{z}(t) := \boldsymbol{y}(t) - \hat{\boldsymbol{y}}(t)$, respectively. Then, motivated by,[29,30] the following virtual reference trajectory is introduced to design the controller:

$$\dot{\boldsymbol{y}}_r := \dot{\boldsymbol{y}}_d - \boldsymbol{\Lambda}\, \boldsymbol{Tanh}(\hat{\boldsymbol{y}} - \boldsymbol{y}_d) = \dot{\boldsymbol{y}}_d - \boldsymbol{\Lambda}\, \boldsymbol{Tanh}(\boldsymbol{e} - \boldsymbol{z}), \tag{16}$$

Then, the following composite error signal is also defined:

$$\boldsymbol{r}_1 := \dot{\boldsymbol{y}} - \dot{\boldsymbol{y}}_r = \dot{\boldsymbol{e}} + \boldsymbol{\Lambda}\, \boldsymbol{Tanh}(\boldsymbol{e} - \boldsymbol{z}), \tag{17}$$

where $\boldsymbol{\Lambda} = \lambda \boldsymbol{I}_3 \in \Re^{3\times 3}$ and $\lambda > 0$. To design the observer, the following signals are also introduced:

$$\dot{\boldsymbol{y}}_o := \dot{\hat{\boldsymbol{y}}} - \boldsymbol{\Lambda}\, \boldsymbol{Tanh}(\boldsymbol{z}), \tag{18}$$

$$\boldsymbol{r}_2 := \dot{\boldsymbol{y}} - \dot{\boldsymbol{y}}_o = \dot{\boldsymbol{z}} + \boldsymbol{\Lambda}\, \boldsymbol{Tanh}(\boldsymbol{z}), \tag{19}$$

By replacing (17) in (15) and applying Property P2.3, one gets

$$\begin{aligned} \boldsymbol{M}_2(\boldsymbol{\eta})\dot{\boldsymbol{r}}_1 = &-\boldsymbol{C}_2(\boldsymbol{\eta},\ \dot{\boldsymbol{y}})\boldsymbol{r}_1 - \boldsymbol{D}_2(\boldsymbol{\eta})\boldsymbol{r}_1 + \boldsymbol{d}(\boldsymbol{\eta}, \boldsymbol{w},\ \dot{\boldsymbol{y}}_r) - \boldsymbol{d}(\boldsymbol{\eta}, \boldsymbol{w},\ \dot{\boldsymbol{y}}) \\ &+ \boldsymbol{J}^{-T}(\boldsymbol{\eta})\boldsymbol{\tau}_a - \boldsymbol{C}_2(\boldsymbol{\eta},\ \dot{\boldsymbol{y}}_r)\boldsymbol{r}_1 + \boldsymbol{\xi}, \end{aligned} \tag{20}$$

where

$$\boldsymbol{\xi} = -\boldsymbol{M}_2(\boldsymbol{\eta})\ddot{\boldsymbol{y}}_r - \boldsymbol{C}_2(\boldsymbol{\eta},\ \dot{\boldsymbol{y}}_r)\dot{\boldsymbol{y}}_r - \boldsymbol{d}(\boldsymbol{\eta}, \boldsymbol{w},\ \dot{\boldsymbol{y}}_r) - \boldsymbol{D}_2(\boldsymbol{\eta})\dot{\boldsymbol{y}}_r - \boldsymbol{G}_2(\boldsymbol{\eta}) - \boldsymbol{\tau}_{w2}(\boldsymbol{\eta}, \boldsymbol{w}, t)$$

represents the uncertain nonlinearities such that $\|\boldsymbol{\xi}\| \leq \rho(\dot{\boldsymbol{y}}_r,\ \ddot{\boldsymbol{y}}_r) = \boldsymbol{G}(\dot{\boldsymbol{y}}_r,\ \ddot{\boldsymbol{y}}_r)\boldsymbol{\theta}$ based on Properties P2.1, P2.4 and P2.5 where $\boldsymbol{G}(\dot{\boldsymbol{y}}_r,\ \ddot{\boldsymbol{y}}_r) = [1\ \ \|\dot{\boldsymbol{y}}_r\|\ \ \|\dot{\boldsymbol{y}}_r\|^2\ \ \|\ddot{\boldsymbol{y}}_r\|]$. Then, the following saturated tracking controller is proposed:

$$\begin{aligned} \boldsymbol{\tau}_a = \boldsymbol{J}^T(\boldsymbol{\eta})(&-\boldsymbol{K}_1\, \boldsymbol{Tanh}(\dot{\boldsymbol{y}}_o - \dot{\boldsymbol{y}}_r) - \boldsymbol{K}_2\, \boldsymbol{Tanh}(\boldsymbol{e} - \boldsymbol{z}) \\ &- \boldsymbol{K}_2\, \boldsymbol{Tanh}(\boldsymbol{z}) - \hat{\rho}(\dot{\boldsymbol{y}}_r,\ \ddot{\boldsymbol{y}}_r)\, \boldsymbol{Tanh}(\nu\hat{\rho}(\hat{\boldsymbol{r}}_1 + \hat{\boldsymbol{r}}_2)/\varepsilon_t)), \end{aligned} \tag{21}$$

where $\hat{\boldsymbol{r}}_1 + \hat{\boldsymbol{r}}_2 := \dot{\hat{\boldsymbol{y}}} - \dot{\boldsymbol{y}}_d + \boldsymbol{\Lambda}\, \boldsymbol{Tanh}(\hat{\boldsymbol{y}} - \boldsymbol{y}_d) + \boldsymbol{\Lambda}\, \boldsymbol{Tanh}(\boldsymbol{z})$, $\boldsymbol{K}_1, \boldsymbol{K}_2 \in \Re^{3\times 3}$ are the positive-definite diagonal gain matrices, $\hat{\rho}(\dot{\boldsymbol{y}}_r,\ \ddot{\boldsymbol{y}}_r) = \boldsymbol{G}(\dot{\boldsymbol{y}}_r,\ \ddot{\boldsymbol{y}}_r)\hat{\boldsymbol{\theta}}$ is an estimation of the upper bounding function $\rho(\dot{\boldsymbol{y}}_r,\ \ddot{\boldsymbol{y}}_r)$, and $\hat{\boldsymbol{\theta}} \in \Re^4$ is updated by the following adaptive law:

$$\dot{\hat{\boldsymbol{\theta}}} = \boldsymbol{\Gamma}\, \boldsymbol{G}^T(\dot{\boldsymbol{y}}_r,\ \ddot{\boldsymbol{y}}_r)\, \|\hat{\boldsymbol{r}}_1 + \hat{\boldsymbol{r}}_2\| - \boldsymbol{\Gamma}\, \boldsymbol{\Sigma}\, (\hat{\boldsymbol{\theta}} - \boldsymbol{\theta}_0), \tag{22}$$

where $\boldsymbol{\Gamma} = \gamma \boldsymbol{I}_4$ shows the adaptation gain, $\boldsymbol{\Sigma} \in \Re^4$ denotes a positive-definite diagonal matrix, and $\boldsymbol{\theta}_0 \in \Re^4$ is *a priori* estimate of the parameters. The following nonlinear saturated observer is also proposed to estimate the velocity of the virtual control point P_R in the front of the AUV in Fig. 1:

$$\dot{\hat{\boldsymbol{y}}}(t) = \dot{\hat{\boldsymbol{y}}}_o(t) + \boldsymbol{\Lambda}\, \boldsymbol{Tanh}(\boldsymbol{z}(t)) + k_d\, \boldsymbol{z}(t), \tag{23}$$

$$\dot{\hat{\boldsymbol{y}}}_o(t) = \dot{\boldsymbol{y}}_r(t) + k_d \boldsymbol{\Lambda} \int_0^t \boldsymbol{Tanh}(\boldsymbol{z}(\tau))\, d\tau, \tag{24}$$

where $k_d \in \Re^+$ is the observer gain. The initial conditions of the observer are chosen as $\dot{\hat{\boldsymbol{y}}}_o(0) = -(\boldsymbol{\Lambda} Tanh(\boldsymbol{z}(0)) + k_d \boldsymbol{z}(0))$, $\hat{\boldsymbol{y}}(0) = \boldsymbol{y}(0)$, $\boldsymbol{z}(0) = 0$ and $\dot{\hat{\boldsymbol{y}}}(0) = 0$.

https://doi.org/10.1017/S0263574717000455 Published online by Cambridge University Press

3.2. Closed-loop error dynamic equations

The closed-loop error dynamic equation is obtained as follows by considering $\boldsymbol{r}_1 - \boldsymbol{r}_2 = \dot{\boldsymbol{y}}_o - \dot{\boldsymbol{y}}_r$ from (17) and (19), and substituting (21) into (20):

$$\begin{aligned}\boldsymbol{M}_2(\boldsymbol{\eta})\dot{\boldsymbol{r}}_1 = &-\boldsymbol{C}_2(\boldsymbol{\eta},\, \dot{\boldsymbol{y}})\boldsymbol{r}_1 - \boldsymbol{D}_2(\boldsymbol{\eta})\boldsymbol{r}_1 - \boldsymbol{K}_1\boldsymbol{Tanh}(\boldsymbol{r}_1 - \boldsymbol{r}_2) - \boldsymbol{K}_2\,\boldsymbol{Tanh}(\boldsymbol{e} - \boldsymbol{z}) \\ &- \boldsymbol{K}_2\,\boldsymbol{Tanh}(\boldsymbol{z}) - \hat{\rho}\boldsymbol{Tanh}(\nu\hat{\rho}(\hat{\boldsymbol{r}}_1 + \hat{\boldsymbol{r}}_2)/\varepsilon_t) + \boldsymbol{\chi}_1 + \boldsymbol{\xi},\end{aligned} \tag{25}$$

where

$$\boldsymbol{\chi}_1 = \boldsymbol{d}(\boldsymbol{\eta},\, \boldsymbol{w},\, \dot{\boldsymbol{y}}_r) - \boldsymbol{d}(\boldsymbol{\eta},\, \boldsymbol{w},\, \dot{\boldsymbol{y}}) - \boldsymbol{C}_2(\boldsymbol{\eta},\, \dot{\boldsymbol{y}}_r)\boldsymbol{r}_1,$$

which is bounded as follows by using $\|\boldsymbol{d}(\boldsymbol{\eta},\, \boldsymbol{w},\, \dot{\boldsymbol{y}}_r) - \boldsymbol{d}(\boldsymbol{\eta},\, \boldsymbol{w},\, \dot{\boldsymbol{y}})\| \leq d_{M1}\|\boldsymbol{r}_1\| + d_{M2}\|\boldsymbol{r}_1\|^2$ from (17) and Property P2.5:

$$\left\|\boldsymbol{\chi}_1\right\| \leq \zeta_1\,\|\boldsymbol{x}\| + \zeta_2\|\boldsymbol{x}\|^2, \tag{26}$$

where $\zeta_1,\ \zeta_2 \in \Re$ are the positive bounding constants and $\boldsymbol{x} \in \Re^{12}$ is defined by

$$\boldsymbol{x} := [\boldsymbol{Tanh}^T(\boldsymbol{e} - \boldsymbol{z}),\ \boldsymbol{Tanh}^T(\boldsymbol{z}),\ \boldsymbol{r}_1^T,\ \boldsymbol{r}_2^T]^T. \tag{27}$$

Since from (23), one can write $\ddot{\boldsymbol{y}} = \ddot{\boldsymbol{y}}_o + \boldsymbol{\Lambda}\,\boldsymbol{Sech}^2(\boldsymbol{z})\dot{\boldsymbol{z}} + k_d\,\dot{\boldsymbol{z}}$, it is very easy to show that (23) and (24) are equivalent to $\dot{\boldsymbol{r}}_1 = \dot{\boldsymbol{r}}_2 + k_d\,\boldsymbol{r}_2$ which together with (25) and Property P2.3 yield the following observer error dynamic equation:

$$\begin{aligned}\boldsymbol{M}_2(\boldsymbol{\eta})\dot{\boldsymbol{r}}_2 = &-\boldsymbol{C}_2(\boldsymbol{\eta},\, \dot{\boldsymbol{y}})\boldsymbol{r}_2 - k_d\boldsymbol{M}_2(\boldsymbol{\eta})\,\boldsymbol{r}_2 - \boldsymbol{K}_1\boldsymbol{Tanh}(\boldsymbol{r}_1 - \boldsymbol{r}_2) - \boldsymbol{K}_2\,\boldsymbol{Tanh}(\boldsymbol{e} - \boldsymbol{z}) \\ &- \boldsymbol{K}_2\,\boldsymbol{Tanh}(\boldsymbol{z}) - \hat{\rho}\boldsymbol{Tanh}(\nu\hat{\rho}(\hat{\boldsymbol{r}}_1 + \hat{\boldsymbol{r}}_2)/\varepsilon_t) + \boldsymbol{\chi}_2 + \boldsymbol{\xi}\end{aligned} \tag{28}$$

where $\boldsymbol{\chi}_2$ is obtained as follows:

$$\boldsymbol{\chi}_2 = \boldsymbol{C}_2(\boldsymbol{\eta},\, \dot{\boldsymbol{y}}_r + \boldsymbol{r}_1)\boldsymbol{r}_2 - \boldsymbol{C}_2(\boldsymbol{\eta}, \boldsymbol{r}_1)(2\dot{\boldsymbol{y}}_r + \boldsymbol{r}_1) - \boldsymbol{D}_2(\boldsymbol{\eta})\boldsymbol{r}_1 + \boldsymbol{d}(\boldsymbol{\eta},\, \boldsymbol{w},\, \dot{\boldsymbol{y}}_r) - \boldsymbol{d}(\boldsymbol{\eta},\, \boldsymbol{w},\, \dot{\boldsymbol{y}})$$

From (16)–(19), Lemma 1, and Properties P2.4, P2.5 and P2.6, the following upper bound holds for $\boldsymbol{\chi}_2$:

$$\left\|\boldsymbol{\chi}_2\right\| \leq \zeta_3\,\|\boldsymbol{x}\| + \zeta_4\|\boldsymbol{x}\|^2, \tag{29}$$

where $\zeta_3,\ \zeta_4 \in \Re$ are the positive bounding constants.

3.3. Stability analysis

The closed-loop stability of the proposed saturated OFB tracking control system is expressed by the following theorem. Then, Lyapunov's direct method is applied to prove the theorem in the sequel.

Theorem 1. Consider the second-order model of underactuated AUVs which is given by (15). Given a bounded continuous desired trajectory, and under Assumptions 1–4, if the gains of the proposed controller (21)–(24) are chosen to meet the following stability conditions:

$$\lambda_{\min}(\boldsymbol{K}_2\boldsymbol{\Lambda}) > 0.5k_{2\max}\lambda + k_{2\max}, \tag{30}$$

$$\lambda_{d_2} > k_{1\max} + 0.5k_{2\max} + 0.5(\zeta_1 + \zeta_2), \tag{31}$$

$$k_d > (2k_{1\max} + k_{2\max} + 0.5(\zeta_3 + \zeta_4))\,/\lambda_{m_2}, \tag{32}$$

where $k_{i\max} = \lambda_{\max}(\boldsymbol{K}_i),\ i = 1, 2$, then, the OFB controller guaranties that all signals of the closed-loop system remain bounded and the tracking and observation errors are semi-globally uniformly ultimately bounded (SGUUB) and converge to a neighborhood of the origin. In addition, the following

https://doi.org/10.1017/S0263574717000455 Published online by Cambridge University Press

region of attraction can be made arbitrarily large to include any initial condition by choosing the control gains large enough:

$$R_A = \left\{ \vartheta \in \Re^{16} \;\middle|\; \|\vartheta\| < \sqrt{\frac{2\alpha_m - (\zeta_1 + \zeta_3)}{(\zeta_2 + \zeta_4)\min\{\lambda_u/\lambda_x,\, 0.5\lambda_{\max}(\boldsymbol{\Gamma}^{-1})/\lambda_x\}}} \right\}, \tag{33}$$

where $\tilde{\boldsymbol{\theta}} = \boldsymbol{\theta} - \hat{\boldsymbol{\theta}}$ denotes the vector of the parameters estimation error, $\vartheta = [\boldsymbol{u}^T,\ \tilde{\boldsymbol{\theta}}^T]^T$, $\boldsymbol{u} = [(\boldsymbol{e} - \boldsymbol{z})^T, \boldsymbol{z}^T,\ \boldsymbol{r}_1^T,\ \boldsymbol{r}_2^T]^T$, α_m is a positive gain-dependent parameter, $\zeta_i,\ i = 1,\ \ldots, 4$ are defined by (26) and (29), $\boldsymbol{x} \in \Re^{12}$ was defined in (27), and λ_x and λ_u will be defined later.

Proof. Consider the following Lyapunov function candidate

$$\begin{aligned} V(t) = {} & \sum_{i=1}^{3} k_{2i} \ln\cosh(e_i - z_i) + \tfrac{1}{2}\boldsymbol{r}_1^T \boldsymbol{M}_2(\boldsymbol{\eta})\boldsymbol{r}_1 + \sum_{i=1}^{3} k_{2i} \ln\cosh(z_i) \\ & + \tfrac{1}{2}\boldsymbol{r}_2^T \boldsymbol{M}_2(\boldsymbol{\eta})\boldsymbol{r}_2 + \tfrac{1}{2}\tilde{\boldsymbol{\theta}}^T \boldsymbol{\Gamma}^{-1}\tilde{\boldsymbol{\theta}} \end{aligned} \tag{34}$$

By using item (i) of Lemma 1, one may confirm that (34) can be bounded as follows:

$$\begin{aligned} & \sum_{i=1}^{3} k_{2i}\tanh^2(e_i - z_i)/2 + \frac{1}{2}\lambda_{m_2}\|\boldsymbol{r}_1\|^2 + \sum_{i=1}^{3} k_{2i}\tanh^2(z_i)/2 + \frac{1}{2}\lambda_{m_2}\|\boldsymbol{r}_2\|^2 + \frac{1}{2}\lambda_{\min}(\boldsymbol{\Gamma}^{-1})\left\|\tilde{\boldsymbol{\theta}}\right\|^2 \\ & \quad \le V(t) \le \lambda_{ks,\max}\|\boldsymbol{e} - \boldsymbol{z}\|^2 + \frac{1}{2}\lambda_{M_2}\|\boldsymbol{r}_1\|^2 + \lambda_{ks,\max}\|\boldsymbol{z}\|^2 + \frac{1}{2}\lambda_{M_2}\|\boldsymbol{r}_2\|^2 + \frac{1}{2}\lambda_{\max}(\boldsymbol{\Gamma}^{-1})\left\|\tilde{\boldsymbol{\theta}}\right\|^2 \end{aligned} \tag{35}$$

which can be stated as follows:

$$\lambda_x\|\boldsymbol{x}\|^2 + 0.5\lambda_{\min}(\boldsymbol{\Gamma}^{-1})\left\|\tilde{\boldsymbol{\theta}}\right\|^2 \le V(t) \le \lambda_u\|\boldsymbol{u}\|^2 + 0.5\lambda_{\max}(\boldsymbol{\Gamma}^{-1})\left\|\tilde{\boldsymbol{\theta}}\right\|^2 \tag{36}$$

where $\lambda_x = \min\{\lambda_{ks,\min},\ \lambda_{m_2}/2\}$, $\lambda_u = \max\{\lambda_{ks,\max}, \lambda_{M_2}/2\}$, $\lambda_{ks,\min} = 0.5\min\{k_{21}, k_{22}, k_{23}\}$, $\lambda_{ks,\max} = 0.5\max\{k_{21}, k_{22}, k_{23}\}$, and λ_{m_2} and λ_{M_2} are defined in Property P2.1. From the above inequality and item (ii) of Lemma 1, it is obvious that $V(t)$ is a positive-definite, decrescent and radially unbounded function. These properties are necessary for the semi-global stability proof. By differentiating (34) along (17), (19), (25) and (28), using Property P2.2 and the fact that $\dot{\hat{\boldsymbol{\theta}}} = -\dot{\tilde{\boldsymbol{\theta}}}$, we get

$$\begin{aligned} \dot{V}(t) = {} & \boldsymbol{Tanh}^T(\boldsymbol{e} - \boldsymbol{z})\boldsymbol{K}_2(\dot{\boldsymbol{e}} - \dot{\boldsymbol{z}}) + \boldsymbol{r}_1^T\boldsymbol{M}_2\dot{\boldsymbol{r}}_1 + \frac{1}{2}\boldsymbol{r}_1^T\dot{\boldsymbol{M}}_2\boldsymbol{r}_1 + \boldsymbol{Tanh}^T(\boldsymbol{z})\boldsymbol{K}_2\dot{\boldsymbol{z}} \\ & + \boldsymbol{r}_2^T\boldsymbol{M}_2\dot{\boldsymbol{r}}_2 + \frac{1}{2}\boldsymbol{r}_2^T\dot{\boldsymbol{M}}_2\boldsymbol{r}_2 - \tilde{\boldsymbol{\theta}}^T\boldsymbol{\Gamma}^{-1}\dot{\hat{\boldsymbol{\theta}}} \\ = {} & -\boldsymbol{Tanh}^T(\boldsymbol{e} - \boldsymbol{z})\boldsymbol{K}_2\boldsymbol{\Lambda}\,\boldsymbol{Tanh}(\boldsymbol{e} - \boldsymbol{z}) - \boldsymbol{Tanh}^T(\boldsymbol{z})\boldsymbol{K}_2\boldsymbol{\Lambda}\,\boldsymbol{Tanh}(\boldsymbol{z}) - \boldsymbol{r}_1^T\boldsymbol{D}_2(\boldsymbol{\eta})\boldsymbol{r}_1 \\ & - k_d\boldsymbol{r}_2^T\boldsymbol{M}_2(\boldsymbol{\eta})\,\boldsymbol{r}_2 - \boldsymbol{r}_1^T\boldsymbol{K}_1\boldsymbol{Tanh}(\boldsymbol{r}_1 - \boldsymbol{r}_2) - \boldsymbol{r}_2^T\boldsymbol{K}_1\boldsymbol{Tanh}(\boldsymbol{r}_1 - \boldsymbol{r}_2) \\ & + \boldsymbol{Tanh}^T(\boldsymbol{e} - \boldsymbol{z})\boldsymbol{K}_2\boldsymbol{\Lambda}\,\boldsymbol{Tanh}(\boldsymbol{z}) - \boldsymbol{r}_1^T\boldsymbol{K}_2\,\boldsymbol{Tanh}(\boldsymbol{z}) - 2\boldsymbol{r}_2^T\boldsymbol{K}_2\,\boldsymbol{Tanh}(\boldsymbol{e} - \boldsymbol{z}) \\ & - \hat{\rho}(\hat{\boldsymbol{r}}_1 + \hat{\boldsymbol{r}}_2)^T\boldsymbol{Tanh}(\nu\hat{\rho}(\hat{\boldsymbol{r}}_1 + \hat{\boldsymbol{r}}_2)/\varepsilon_t) + \boldsymbol{r}_1^T\boldsymbol{\chi}_1 + \boldsymbol{r}_2^T\boldsymbol{\chi}_2 + (\boldsymbol{r}_1 + \boldsymbol{r}_2)^T\boldsymbol{\xi} - \tilde{\boldsymbol{\theta}}^T\boldsymbol{\Gamma}^{-1}\dot{\hat{\boldsymbol{\theta}}} \end{aligned} \tag{37}$$

After re-arrangement, considering $\hat{\boldsymbol{r}}_1 + \hat{\boldsymbol{r}}_2 \cong \boldsymbol{r}_1 + \boldsymbol{r}_2$ from Remark 5 in the next section, and adding and subtracting $\boldsymbol{r}_1^T\boldsymbol{K}_1\boldsymbol{Tanh}(\boldsymbol{r}_1)$ and $\boldsymbol{r}_2^T\boldsymbol{K}_1\boldsymbol{Tanh}(\boldsymbol{r}_1)$, (37) is re-written as follows:

$$\begin{aligned} \dot{V}(t) \le {} & -\boldsymbol{Tanh}^T(\boldsymbol{e} - \boldsymbol{z})\boldsymbol{K}_2\boldsymbol{\Lambda}\,\boldsymbol{Tanh}(\boldsymbol{e} - \boldsymbol{z}) - \boldsymbol{Tanh}^T(\boldsymbol{z})\boldsymbol{K}_2\boldsymbol{\Lambda}\,\boldsymbol{Tanh}(\boldsymbol{z}) \\ & - \boldsymbol{r}_1^T\boldsymbol{D}_2(\boldsymbol{\eta})\boldsymbol{r}_1 - k_d\boldsymbol{r}_2^T\boldsymbol{M}_2(\boldsymbol{\eta})\,\boldsymbol{r}_2 - \boldsymbol{r}_1^T\boldsymbol{K}_1\boldsymbol{Tanh}(\boldsymbol{r}_1) \\ & + \|\boldsymbol{K}_1\|\,\|\boldsymbol{r}_1\|\,\|\boldsymbol{Tanh}(\boldsymbol{r}_1) - \boldsymbol{Tanh}(\boldsymbol{r}_1 - \boldsymbol{r}_2)\| - \boldsymbol{r}_2^T\boldsymbol{K}_1\boldsymbol{Tanh}(\boldsymbol{r}_1) \\ & + \|\boldsymbol{K}_1\|\,\|\boldsymbol{r}_2\|\,\|\boldsymbol{Tanh}(\boldsymbol{r}_1) - \boldsymbol{Tanh}(\boldsymbol{r}_1 - \boldsymbol{r}_2)\| + \|\boldsymbol{K}_2\|\,\|\boldsymbol{r}_1\|\,\|\boldsymbol{Tanh}(\boldsymbol{z})\| \\ & + \|\boldsymbol{K}_2\boldsymbol{\Lambda}\|\,\|\boldsymbol{Tanh}(\boldsymbol{e} - \boldsymbol{z})\|\,\|\boldsymbol{Tanh}(\boldsymbol{z})\| + 2\,\|\boldsymbol{K}_2\|\,\|\boldsymbol{r}_2\|\,\|\boldsymbol{Tanh}(\boldsymbol{e} - \boldsymbol{z})\| \\ & + \|\boldsymbol{r}_1\|\,\left\|\boldsymbol{\chi}_1\right\| + \|\boldsymbol{r}_2\|\,\left\|\boldsymbol{\chi}_2\right\| + \|\boldsymbol{r}_1 + \boldsymbol{r}_2\|\,\|\boldsymbol{\xi}\| - \tilde{\boldsymbol{\theta}}^T\boldsymbol{\Gamma}^{-1}\dot{\hat{\boldsymbol{\theta}}} \\ & - \hat{\rho}(\boldsymbol{r}_1 + \boldsymbol{r}_2)^T\boldsymbol{Tanh}(\nu\hat{\rho}(\boldsymbol{r}_1 + \boldsymbol{r}_2)/\varepsilon_t) \end{aligned} \tag{38}$$

https://doi.org/10.1017/S0263574717000455 Published online by Cambridge University Press

By recalling the adaptive law (22), taking items (iii), (iv) and (v) of Lemma 1 into account, and recalling the upper bounds on $\|\boldsymbol{\xi}\|$,$\|\boldsymbol{\chi}_1\|$ and $\|\boldsymbol{\chi}_2\|$, one achieves

$$\begin{aligned}\dot{V}(t) \leq & -\lambda_{\min}(\boldsymbol{K}_2\boldsymbol{\Lambda})\,\|\boldsymbol{Tanh}(\boldsymbol{e}-\boldsymbol{z})\|^2 - \lambda_{\min}(\boldsymbol{K}_2\boldsymbol{\Lambda})\,\|\boldsymbol{Tanh}(\boldsymbol{z})\|^2 - \lambda_{d_2}\|\boldsymbol{r}_1\|^2 \\ & - \lambda_{\min}(k_d\boldsymbol{M}_2(\boldsymbol{\eta}))\|\boldsymbol{r}_2\|^2 + \|\boldsymbol{K}_1\|\,\|\boldsymbol{r}_1\|\,\|\boldsymbol{r}_2\| - \lambda_{\min}(\boldsymbol{K}_1)\|\boldsymbol{Tanh}(\boldsymbol{r}_1)\|^2 \\ & + \|\boldsymbol{K}_1\|\,\|\boldsymbol{r}_2\|^2 + \|\boldsymbol{K}_1\|\,\|\boldsymbol{r}_1\|\,\|\boldsymbol{r}_2\| + \|\boldsymbol{K}_2\boldsymbol{\Lambda}\|\,\|\boldsymbol{Tanh}(\boldsymbol{e}-\boldsymbol{z})\|\,\|\boldsymbol{Tanh}(\boldsymbol{z})\| \\ & + \|\boldsymbol{K}_2\|\,\|\boldsymbol{r}_1\|\,\|\boldsymbol{Tanh}(\boldsymbol{z})\| + 2\,\|\boldsymbol{K}_2\|\,\|\boldsymbol{r}_2\|\,\|\boldsymbol{Tanh}(\boldsymbol{e}-\boldsymbol{z})\| + \zeta_1\,\|\boldsymbol{r}_1\|\,\|\boldsymbol{x}\| \\ & + \zeta_2\,\|\boldsymbol{r}_1\|\,\|\boldsymbol{x}\|^2 + \zeta_3\,\|\boldsymbol{r}_2\|\,\|\boldsymbol{x}\| + \zeta_4\,\|\boldsymbol{r}_2\|\,\|\boldsymbol{x}\|^2 - \hat{\rho}(\boldsymbol{r}_1+\boldsymbol{r}_2)^T\boldsymbol{Tanh}(\nu\hat{\rho}(\boldsymbol{r}_1+\boldsymbol{r}_2)/\varepsilon_t) \\ & + \|\boldsymbol{r}_1+\boldsymbol{r}_2\|\,\boldsymbol{G}(\dot{\boldsymbol{y}}_r,\,\ddot{\boldsymbol{y}}_r)\boldsymbol{\theta} - \tilde{\boldsymbol{\theta}}^T\boldsymbol{G}^T(\dot{\boldsymbol{y}}_r,\,\ddot{\boldsymbol{y}}_r)\,\|\boldsymbol{r}_1+\boldsymbol{r}_2\| + \tilde{\boldsymbol{\theta}}^T\boldsymbol{\Sigma}(\hat{\boldsymbol{\theta}}-\boldsymbol{\theta}_0)\end{aligned} \tag{39}$$

By considering $\hat{\boldsymbol{\theta}} = \boldsymbol{\theta} - \tilde{\boldsymbol{\theta}}$, applying Lemma 2, recalling Young's inequality $\|\boldsymbol{K}\|\|\boldsymbol{x}_1\|\|\boldsymbol{x}_2\| \leq 0.5\lambda_{\max}(\boldsymbol{K})\|\boldsymbol{x}_1\|^2 + 0.5\lambda_{\max}(\boldsymbol{K})\|\boldsymbol{x}_2\|^2$, $\forall \boldsymbol{x}_1,\ \boldsymbol{x}_2 \in \Re^n$, and considering

$$\begin{aligned}& 2\,\|\boldsymbol{K}_1\|\,\|\boldsymbol{r}_1\|\,\|\boldsymbol{r}_2\| \leq k_{1\max}\|\boldsymbol{r}_1\|^2 + k_{1\max}\|\boldsymbol{r}_2\|^2, \\ & \|\boldsymbol{K}_2\Lambda\|\,\|\boldsymbol{Tanh}(\boldsymbol{e}-\boldsymbol{z})\|\,\|\boldsymbol{Tanh}(\boldsymbol{z})\| \leq 0.5k_{2\max}\lambda\,\|\boldsymbol{Tanh}(\boldsymbol{e}-\boldsymbol{z})\|^{\,2} + 0.5k_{2\max}\lambda\,\|\boldsymbol{Tanh}(\boldsymbol{z})\|^2, \\ & \|\boldsymbol{K}_2\|\,\|\boldsymbol{r}_1\|\,\|\boldsymbol{Tanh}(\boldsymbol{z})\| \leq 0.5k_{2\max}\,\|\boldsymbol{r}_1\|^{\,2} + 0.5k_{2\max}\|\boldsymbol{Tanh}(\boldsymbol{z})\|^2, \\ & 2\,\|\boldsymbol{K}_2\|\,\|\boldsymbol{r}_2\|\,\|\boldsymbol{Tanh}(\boldsymbol{e}-\boldsymbol{z})\| \leq k_{2\max}\,\|\boldsymbol{r}_2\|^{\,2} + k_{2\max}\|\boldsymbol{Tanh}(\boldsymbol{e}-\boldsymbol{z})\|^2, \\ & \|\boldsymbol{r}_1+\boldsymbol{r}_2\|\,\boldsymbol{G}(\dot{\boldsymbol{y}}_r,\,\ddot{\boldsymbol{y}}_r)\hat{\boldsymbol{\theta}} - \hat{\rho}(\boldsymbol{r}_1+\boldsymbol{r}_2)^T\boldsymbol{Tanh}(\nu\hat{\rho}(\boldsymbol{r}_1+\boldsymbol{r}_2)/\varepsilon_t) \leq 3\varepsilon_t\end{aligned}$$

one may express (39) as

$$\begin{aligned}\dot{V}(t) \leq & -\alpha_1\,\|\boldsymbol{Tanh}(\boldsymbol{e}-\boldsymbol{z})\|^2 - \alpha_2\,\|\boldsymbol{Tanh}(\boldsymbol{z})\|^2 - \alpha_3\|\boldsymbol{r}_1\|^2 - \alpha_4\|\boldsymbol{r}_2\|^2 - \lambda_{\min}(\boldsymbol{K}_1)\|\boldsymbol{Tanh}(\boldsymbol{r}_1)\|^2 \\ & +0.5(\zeta_1+\zeta_3)\|\boldsymbol{x}\|^2 + 0.5(\zeta_2+\zeta_4)\|\boldsymbol{x}\|^4 + 3\varepsilon_t + \tilde{\boldsymbol{\theta}}^T\boldsymbol{\Sigma}\,(\hat{\boldsymbol{\theta}}-\boldsymbol{\theta}_0),\end{aligned} \tag{40}$$

where the parameters $\alpha_i,\ i = 1,\ \ldots, 4$ are defined as $\alpha_1 = \lambda_{\min}(\boldsymbol{K}_2\boldsymbol{\Lambda}) - 0.5k_{2\max}\lambda - k_{2\max}$, $\alpha_2 = \lambda_{\min}(\boldsymbol{K}_2\boldsymbol{\Lambda}) - 0.5k_{2\max}\lambda - 0.5k_{2\max}$, $\alpha_3 = \lambda_{d_2} - k_{1\max} - 0.5k_{2\max} - 0.5(\zeta_1+\zeta_2)$, and $\alpha_4 = k_d\lambda_{m_2} - 2k_{1\max} - k_{2\max} - 0.5(\zeta_3+\zeta_4)$. The control gains should be chosen such that $\alpha_i > 0,\ i = 1, \ldots, 4$, which, in turn, lead to the conditions (30)–(32). By completing the square terms in the last term of (40), it is written as follows:

$$\begin{aligned}\dot{V}(t) &\leq -\alpha_m\|\boldsymbol{x}\|^2 + 0.5(\zeta_1+\zeta_3)\|\mathbf{x}\|^2 + 0.5(\zeta_2+\zeta_4)\|\boldsymbol{x}\|^4 \\ &\quad - \lambda_{\min}(\boldsymbol{K}_1)\|\boldsymbol{Tanh}(\boldsymbol{r}_1)\|^2 - \mu_\sigma(1-0.5/\kappa^2)\left\|\tilde{\boldsymbol{\theta}}\right\|^2 + \gamma(t) \\ &\leq -(\alpha_m - 0.5(\zeta_1+\zeta_3) - 0.5(\zeta_2+\zeta_4)\|\boldsymbol{x}\|^2)\|\boldsymbol{x}\|^2 \\ &\quad - \mu_\sigma(1-0.5/\kappa^2)\left\|\tilde{\boldsymbol{\theta}}\right\|^2 + \gamma(t)\end{aligned} \tag{41}$$

where $\boldsymbol{x} \in \Re^{12}$ is defined by (27) and $\alpha_m = \min\{\alpha_1,\ \alpha_2, \alpha_3, \alpha_4\}$, $\gamma(t) = 0.5\mu_\sigma\kappa^2||\boldsymbol{\theta}-\boldsymbol{\theta}_0||^2 + 3\varepsilon_t(t)$, $\mu_\sigma = \sqrt{\lambda_{\min}(\boldsymbol{\Sigma}^T\boldsymbol{\Sigma})}$ and $\kappa \in \Re^+$ where $\kappa > \sqrt{2}/2$. Hence, if α_m is selected such that

$$\alpha_m > 0.5(\zeta_1+\zeta_3) + 0.5(\zeta_2+\zeta_4)\|\mathbf{x}\|^2, \tag{42}$$

Then, (41) can be stated as

$$\dot{V}(t) \leq -c_m\|\boldsymbol{x}\|^2 - \mu_\sigma(1-0.5/\kappa^2)\left\|\tilde{\boldsymbol{\theta}}\right\|^2 + \gamma(t), \tag{43}$$

where $c_m \in \Re$ is a positive constant. The inequality (43) is also expressed as follows:

$$\dot{V}(t) \leq -c\|\boldsymbol{p}(t)\|^2 + \gamma(t) \tag{44}$$

where $c = \min\{c_m,\ \mu_\sigma(1-0.5/\kappa^2)\}$ is also a positive scalar constant, and $\boldsymbol{p}(t) \in \Re^{16}$ is given by $\boldsymbol{p}(t) = [\boldsymbol{x}^T(t),\ \tilde{\boldsymbol{\theta}}^T(t)]^T$. Therefore, provided that conditions (30)–(32), and (42) are satisfied, $\dot{V}(t)$ is strictly negative outside the compact set $\boldsymbol{\Omega}_p = \{\boldsymbol{p}(t) \mid 0 \leq \|\boldsymbol{p}(t)\| \leq \sqrt{\gamma/c}\}$. This expression points

https://doi.org/10.1017/S0263574717000455 Published online by Cambridge University Press

out that $V(t)$ is decreasing outside the set $\boldsymbol{\Omega}_p$ which results in the following inequality

$$V(t) \leq V(0) \leq \lambda_u \|\boldsymbol{u}(0)\|^2 + 0.5\lambda_{\max}(\boldsymbol{\Gamma}^{-1})\left\|\tilde{\theta}(0)\right\|^2 \ \forall t \geq 0 \tag{45}$$

where the upper bound on $V(t)$ in (36) has been used. From (45) and (36), one gets

$$\|\boldsymbol{x}\|^2 \leq \lambda_u/\lambda_x \|\boldsymbol{u}(0)\|^2 + 0.5\lambda_{\max}(\boldsymbol{\Gamma}^{-1})/\lambda_x \left\|\tilde{\boldsymbol{\theta}}(0)\right\|^2. \tag{46}$$

Thus, a sufficient condition for (42) is given by

$$\alpha_m > 0.5(\zeta_1 + \zeta_3) + 0.5(\zeta_2 + \zeta_4)(\lambda_u/\lambda_x \|\boldsymbol{u}(0)\|^2 + 0.5\lambda_{\max}(\boldsymbol{\Gamma}^{-1})/\lambda_x \left\|\tilde{\boldsymbol{\theta}}(0)\right\|^2), \tag{47}$$

This inequality shows that we can make the region of attraction in (33) arbitrarily large in order to include any initial condition by choosing the control gains large enough. As a result, $\|\boldsymbol{p}(t)\|$ is SGUUB. By considering the properties of the saturation functions, this result indicates that $\boldsymbol{e}(t) - \boldsymbol{z}(t), \boldsymbol{z}(t), \boldsymbol{r}_1(t), \boldsymbol{r}_2(t), \tilde{\boldsymbol{\theta}}(t) \in L_\infty$ which results in $\boldsymbol{e}(t) \in L_\infty$. The above discussion proves that the tracking errors, state estimation errors and parameter estimation errors are SGUUB. Therefore, by taking (17) and (19) into account, one concludes that $\dot{\boldsymbol{e}}(t), \dot{\boldsymbol{z}}(t) \in L_\infty$. Finally, one obtains $\boldsymbol{\eta}(t), \boldsymbol{\upsilon}(t), \hat{\boldsymbol{\upsilon}}(t), \hat{\boldsymbol{\theta}}(t), \boldsymbol{\tau}_a(t) \in L_\infty$ by considering (9), (10), the control (21), and Assumptions 1 and 4. This completes the proof.

3.4. Remarks

Reamrk 3. Considering the definition of $\dot{\boldsymbol{y}}_r(t)$ in (16) and the observer definition in (23) and (24), the signal $\ddot{\boldsymbol{y}}_r = \ddot{\boldsymbol{y}}_d - \boldsymbol{\Lambda}\, \boldsymbol{Sech}^2(\hat{\boldsymbol{y}} - \boldsymbol{y}_d)(\dot{\hat{\boldsymbol{y}}} - \dot{\boldsymbol{y}}_d)$ is available for the computation of $\hat{\rho}(\dot{\boldsymbol{y}}_r, \ \ddot{\boldsymbol{y}}_r)$ in the proposed controller in (21).

Reamrk 4. The conditions (30)–(32) in Theorem 1 present the sufficient conditions of the stability of the closed-loop system which are the result of a conservative Lyapunov-based stability analysis. One may find less restrictive sufficient conditions on the control gains in a similar stability proof. In addition, the presented stability conditions will not be required for the controller implementation. It should be noted that since the energy dissipation elements in AUV dynamics such as potential damping, skin friction, wave drift damping, and damping due to the vortex shedding always exist in practice, the condition (31) is not restrictive for the proposed controller.

Reamrk 5. One can easily confirm that the use of the approximation $\hat{\boldsymbol{r}}_1 + \hat{\boldsymbol{r}}_2 \cong \boldsymbol{r}_1 + \boldsymbol{r}_2$ in (38) is reasonable when observer-controller gains k_d and $\boldsymbol{\Lambda}$ are chosen large enough. The interested reader is referred to ref. [30] for a detailed discussion.

Reamrk 6. The controller-observer parameters $\boldsymbol{\Lambda}, \boldsymbol{K}_1, \boldsymbol{K}_2, k_d, \boldsymbol{\Gamma}, \boldsymbol{\Sigma}$ and $\boldsymbol{\theta}_0$ may be tuned to adjust the convergence rate c and the size of the ultimate bound γ/c. For the example, the following tuning rules can be deduced from the above stability analysis which help the user to adjust all control parameters properly: (i) by considering the definitions of $\alpha_i, \ i = 1, \ \ldots, 4$ after (40), the larger values of $\boldsymbol{\Lambda}, \boldsymbol{K}_2, k_d$, increase c and decrease the size of the ultimate bound γ/c; (ii) the smaller values of $\boldsymbol{\Sigma}$ decrease the value of γ and consequently leads to the smaller ultimate bound γ/c; (iii) the time function $\epsilon_t(t)$ in the saturation-type controller $\boldsymbol{Tanh}(\bullet)$ in (21) may be tuned to compromise between the final tracking accuracy and the smoothness of the control signal. The controller (21) may be made smoother by choosing a larger value for $\epsilon_t(t)$. However, the larger value of $\epsilon_t(t)$ increases the value of $\gamma(t)$ in (44) which may result in a larger ultimate bound.

3.5. A generalization

In this section, the proposed controller is generalized to a more general class of strictly increasing continuously differentiable saturation functions which are denoted by $s_i(\bullet)$ according to Definition 2. By defining the vectors $\boldsymbol{s}(\boldsymbol{\eta}) := [s_1(\eta_1), \ s_2(\eta_2), \ \ldots, \ s_n(\eta_n)]^T$ and $\boldsymbol{S}'(\boldsymbol{\eta}) = \text{diag}[s_1'(\eta_1), \ \ldots, \ s_n'(\eta_n)]$, with $\|\boldsymbol{S}'(\boldsymbol{\eta})\| \leq s'_{MM}, \ \forall \boldsymbol{\eta} \in \Re^n$, and introducing the following definitions $\dot{\boldsymbol{y}}_r := \dot{\boldsymbol{y}}_d - \boldsymbol{\Lambda}\, \boldsymbol{s}(\boldsymbol{e} - \boldsymbol{z})$, $\boldsymbol{r}_1 := \dot{\boldsymbol{y}} - \dot{\boldsymbol{y}}_r = \dot{\boldsymbol{e}} + \boldsymbol{\Lambda}\, \boldsymbol{s}(\boldsymbol{e} - \boldsymbol{z}), \ \dot{\boldsymbol{y}}_o := \dot{\hat{\boldsymbol{y}}} - \boldsymbol{\Lambda}\, \boldsymbol{s}(\boldsymbol{z})$, and $\boldsymbol{r}_2 := \dot{\boldsymbol{y}} - \dot{\boldsymbol{y}}_o = \dot{\boldsymbol{z}} + \boldsymbol{\Lambda}\, \boldsymbol{s}(\boldsymbol{z})$, the following theorem can be proven.

https://doi.org/10.1017/S0263574717000455 Published online by Cambridge University Press

Theorem 2. Consider the reduced model of the AUV in (15) again. Given a bounded continuous desired trajectory, and under Assumptions 1–4, the following adaptive tracking controller

$$\begin{aligned}\boldsymbol{\tau}_a = \boldsymbol{J}^T(\boldsymbol{\eta})(&-\boldsymbol{K}_1\, \boldsymbol{s}(\dot{\boldsymbol{y}}_o - \dot{\boldsymbol{y}}_r) - \boldsymbol{K}_2\, \boldsymbol{s}(\boldsymbol{e} - \boldsymbol{z}) \\ &- \boldsymbol{K}_2\, \boldsymbol{s}(\boldsymbol{z}) - \hat{\rho}(\dot{\boldsymbol{y}}_r,\ \ddot{\boldsymbol{y}}_r)\, \boldsymbol{Tanh}(\nu\hat{\rho}(\hat{\boldsymbol{r}}_1 + \hat{\boldsymbol{r}}_2)/\varepsilon_t)),\end{aligned} \tag{48}$$

$$\dot{\hat{\boldsymbol{\theta}}} = \boldsymbol{\Gamma}\, \boldsymbol{G}^T(\dot{\boldsymbol{y}}_r,\ \ddot{\boldsymbol{y}}_r)\, \|\hat{\boldsymbol{r}}_1 + \hat{\boldsymbol{r}}_2\| - \boldsymbol{\Gamma}\, \boldsymbol{\Sigma}\, (\hat{\boldsymbol{\theta}} - \boldsymbol{\theta}_0), \tag{49}$$

with the observer definition

$$\dot{\hat{\boldsymbol{y}}}(t) = \dot{\hat{\boldsymbol{y}}}_o(t) + \boldsymbol{\Lambda}\, \boldsymbol{s}(\boldsymbol{z}(t)) + k_d \boldsymbol{z}(t), \tag{50}$$

$$\ddot{\hat{\boldsymbol{y}}}_o(t) = \ddot{\boldsymbol{y}}_r(t) + k_d \boldsymbol{\Lambda} s(\boldsymbol{z}(t)), \tag{51}$$

under the following gain conditions

$$\lambda_{\min}(\boldsymbol{K}_2\boldsymbol{\Lambda}) > 0.5k_{2\max}\lambda + k_{2\max}, \tag{52}$$

$$\lambda_{d_2} > s'_{MM}k_{1\max} + 0.5k_{2\max} + 0.5(\zeta_1 + \zeta_2), \tag{53}$$

$$k_d > \left(2s'_{MM}k_{1\max} + k_{2\max} + 0.5(\zeta_3 + \zeta_4)\right)/\lambda_{m_2}, \tag{54}$$

guarantee that all signals in the closed-loop system are bounded and the tracking and observation errors are SGUUB and converge to a small ball containing the origin. Moreover, the region of attraction (33) can be made arbitrarily large to include any initial condition by selecting the control gains large enough.

Proof. By constructing the following Lyapunov function candidate

$$\begin{aligned}V(t) = &\sum_{i=1}^{3} k_{2i} \int_0^{e_i - z_i} s_i(r)\, dr + \frac{1}{2}\boldsymbol{r}_1^T \boldsymbol{M}_2(\boldsymbol{\eta})\boldsymbol{r}_1 + \sum_{i=1}^{3} k_{2i} \int_0^{z_i} s_i(r)\, dr \\ &+ \frac{1}{2}\boldsymbol{r}_2^T \boldsymbol{M}_2(\boldsymbol{\eta})\boldsymbol{r}_2 + \frac{1}{2}\tilde{\boldsymbol{\theta}}^T \boldsymbol{\Gamma}^{-1}\tilde{\boldsymbol{\theta}},\end{aligned} \tag{55}$$

the proof is accomplished similar to the proof of Theorem 1 by using Lemma 1. Therefore, the proof is omitted here to save the space of this paper and it is left to the interested readers.

Fig. 2 shows a block diagram of the proposed control system.

4. Numerical Simulations

4.1. Trajectory tracking for a single AUV

Some numerical simulations have been performed to illustrate the effectiveness of the proposed controller. The simulation results are depicted in this section. All of simulations are carried out by using MATLAB software. In order to simulate a more realistic AUV, 6-DOF kinematic and dynamic models of AUVs are considered from.[21] The roll interaction is taken into account as an external disturbance in this paper. A Gaussian white noise is also added to the output measurements by using *randn*(•) function to simulate a localization system. All of simulations are performed based on Euler approximation with a time step of 20 msec. It is assumed that the AUV is equipped with some propellers to provide the surge force, pitch and yaw moments. The AUV parameters are selected as $m_{11} = 25\,\text{kg}$, $m_{22} = 17.5\,\text{kg}$, $m_{33} = 30\,\text{kg}$, $m_{44} = 22.5\,\text{kgm}^2$, $m_{55} = 22.5\,\text{kgm}^2$, $m_{66} = 15\,\text{kgm}^2$, $d_{kk} = 30\,\text{kgs}^{-1}$, $k = 1, 2, 3$, $d_{kk} = 20\,\text{kgm}^2\text{s}^{-1}$, $k = 4, 5, 6$, $\rho g \nabla G M_L = 5$, and $\ell = 0.35\,\text{m}$ for this simulation. In addition, the control signals are saturated such that $|\tau_k| \leq 80\,\text{Nm}$, $k = u, q, r$ to simulate the real actuators. It is assumed that AUV parameters including the mass, the moment of inertia and the damping coefficients are unknown in practice. Moreover, the environmental disturbances, which are

https://doi.org/10.1017/S0263574717000455 Published online by Cambridge University Press

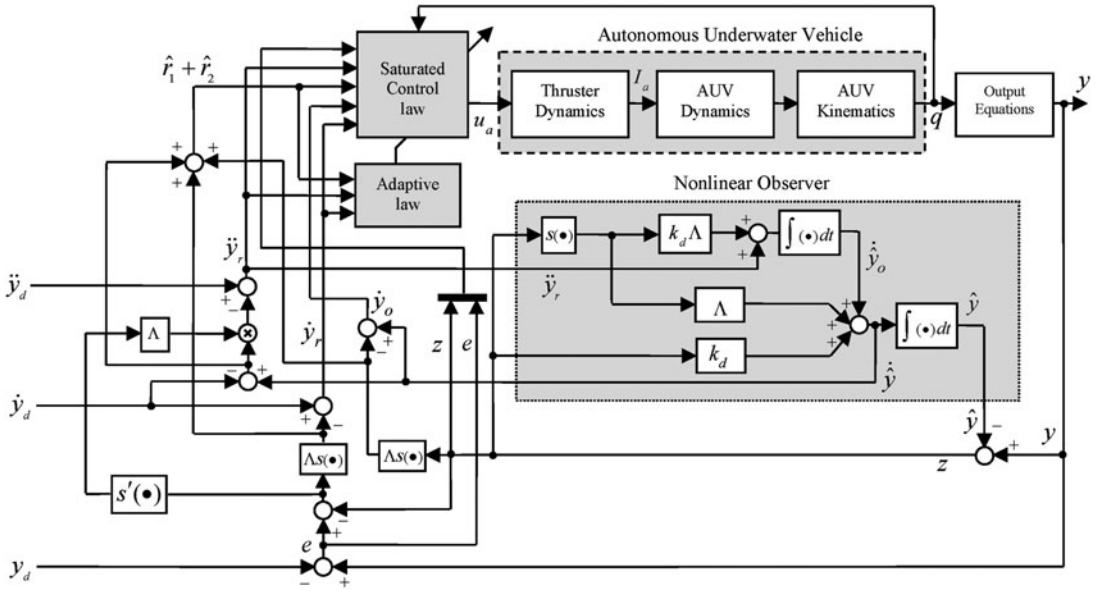

Fig. 2. A block diagram of the proposed saturated output feedback control system.

induced by the friction, waves, and ocean currents, are simulated as follows in all degrees of freedom:

$$\tau_{wk}(t) = A_f \text{sign}(k) + A_d \sin(\omega_d t), \quad k = u, v, w, p, q, r \tag{56}$$

where A_f, A_d and ω_d represent the amplitudes and the frequency of disturbance signals. In order to verify the AUV model and its attributed parameters for this simulation, some open-loop simulation tests have been performed under constant torque inputs.

Fig. 3(a) shows the AUV trajectory, surge velocity and acceleration signals under $\tau_u = 10\,\text{N}$, $\tau_q = 0\,\text{Nm}$ and $\tau_r = 0\,\text{Nm}$. Figure 3(b) illustrates the AUV performance under $\tau_u = 20\,\text{N}$, $\tau_q = 2\,\text{Nm}$ and $\tau_r = 4\,\text{Nm}$. From Fig. 3, it is obvious that the response of the simulated model is consistent with a real AUV. In addition, the minimum turning radius of AUV manoeuvring is 0.6 m for the maximum constant surge force and yaw torque. In order to simulate the proposed closed-loop controller, the control parameters are chosen as $\boldsymbol{K}_1 = 10\boldsymbol{I}_3$, $\boldsymbol{K}_2 = 10\boldsymbol{I}_3$, $\lambda = 1$, $k_d = 50$, $\boldsymbol{\Gamma} = \boldsymbol{I}_4$, $\boldsymbol{\Sigma} = 0.001\boldsymbol{I}_4$, $\boldsymbol{\theta}_0 = \boldsymbol{0}$ and $\varepsilon_t = 1$. The parameters of the disturbance signals in (56) are selected as $A_f = 0.5$, $A_d = 1$ and $\omega_d = 0.1$. The initial posture (the position and orientation) of the AUV is set to $x(0) = 2.0\,\text{m}$, $y(0) = 6.0\,\text{m}$, $z(0) = 0.0\,\text{m}$, $\theta(0) = 0$ rad, and $\psi(0) = 0$ rad for this simulation. The reference trajectory $\mathbf{y}_d(t)$ is generated by an open-loop motion planner whose initial posture is set to $x_d(0) = 0\,\text{m}$, $y_d(0) = 0\,\text{m}$, $z_d(0) = -2.0\,\text{m}$, $\theta_d(0) = 0$ rad, and $\psi_d(0) = 0$ rad. To drive the motion planner in a helical trajectory, the following torque inputs are applied: $\tau_{ud} = 5\,\text{N}$, $\tau_{qd} = 1\,\text{Nm}$ and $\tau_{rd} = 2\,\text{Nm}$. In this simulation, the helical trajectories are selected for the AUV motion to excite the nonlinear dynamics of the vehicle including Coriolis and centripetal forces for an efficient evaluation of the proposed controller performance. In addition, the AUV may employ a helical trajectory to descend in the depth for the sea exploration, oceanographic mapping, ocean floor survey and deep sea archaeology for the example in practice. Figure 4 illustrates the tracking results including x-y-z plot, output tracking errors, control signals and estimated parameters for the proposed controller. As shown by the figure, the AUV successfully tracks the desired trajectory without the actuator saturation. The estimated parameters are bounded and the tracking errors exponentially converge to a neighborhood of the origin. A clear advantage of the proposed controller is that it shows a smooth transient response. As shown by the figure, the generated control signals lie within the acceptable saturating bounds.

4.2. A performance evaluation

This section plans to compare the proposed controller with an adaptive robust PD controller which is a traditional solution for the position control of many robotic systems in Euler-Lagrange form (15). The choice of the adaptive robust PD controller in this comparison is useful to evaluate the ability

https://doi.org/10.1017/S0263574717000455 Published online by Cambridge University Press

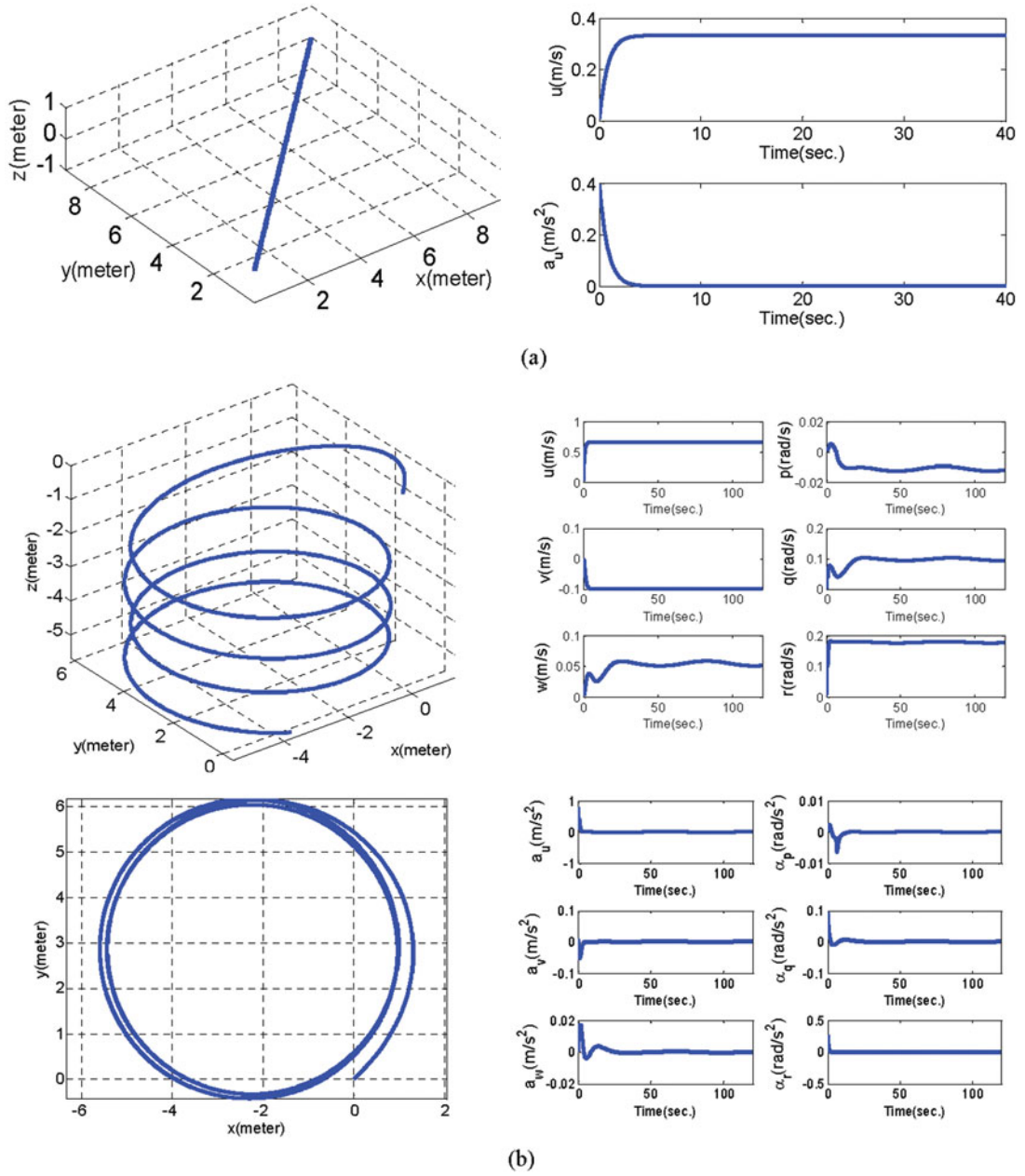

Fig. 3. Open-loop simulation results: (a) *x*–*y*–*z* plot, surge velocity and acceleration under constant surge force, (b) *x*–*y*–*z* plot, *x*–*y* plot, AUV velocities and accelerations under constant surge force, pitch and yaw torques.

of the proposed controller in reducing the risk of the actuator saturation. The adaptive robust PD controller is designed as follows by using the results of:[26]

$$\boldsymbol{\tau}_a = \boldsymbol{J}^T(\boldsymbol{\eta})(-\boldsymbol{K}_1\,\boldsymbol{r}(t) - \hat{\rho}(\dot{\boldsymbol{y}}_d,\ \ddot{\boldsymbol{y}}_d)\,\boldsymbol{Tanh}(\nu\hat{\rho}\boldsymbol{r}(t)/\varepsilon_t)), \tag{57}$$

where $\boldsymbol{r}(t) = \dot{\boldsymbol{e}}(t) + \boldsymbol{\Lambda}e(t)$ is a filtered error signal, $\boldsymbol{\Lambda} = \lambda \boldsymbol{I}_3 \in \Re^{3\times 3}$ and $\boldsymbol{K}_1 \in \Re^{3\times 3}$ denote the control gain matrices, $\hat{\rho}(\dot{\boldsymbol{y}}_d,\ \ddot{\boldsymbol{y}}_d) = \boldsymbol{G}(\dot{\boldsymbol{y}}_d,\ \ddot{\boldsymbol{y}}_d)\hat{\boldsymbol{\theta}}$, $\boldsymbol{G}(\dot{\boldsymbol{y}}_d,\ \ddot{\boldsymbol{y}}_d) = [1,\ \|\dot{\boldsymbol{y}}_d\|,\ \|\dot{\boldsymbol{y}}_d\|^2,\ \|\ddot{\boldsymbol{y}}_d\|]$ and $\hat{\boldsymbol{\theta}}$ is updated by the following adaptive rule:

$$\dot{\hat{\boldsymbol{\theta}}} = \boldsymbol{\Gamma}\,\boldsymbol{G}^T(\dot{\boldsymbol{y}}_d,\ \ddot{\boldsymbol{y}}_d)\,\|\boldsymbol{r}(t)\| - \boldsymbol{\Gamma}\,\boldsymbol{\Sigma}\,(\hat{\boldsymbol{\theta}} - \boldsymbol{\theta}_0). \tag{58}$$

For a fair comparison, the same simulation parameters are chosen for both controllers similar to the previous simulation parameters. However, the initial posture of the open-loop motion planner

https://doi.org/10.1017/S0263574717000455 Published online by Cambridge University Press

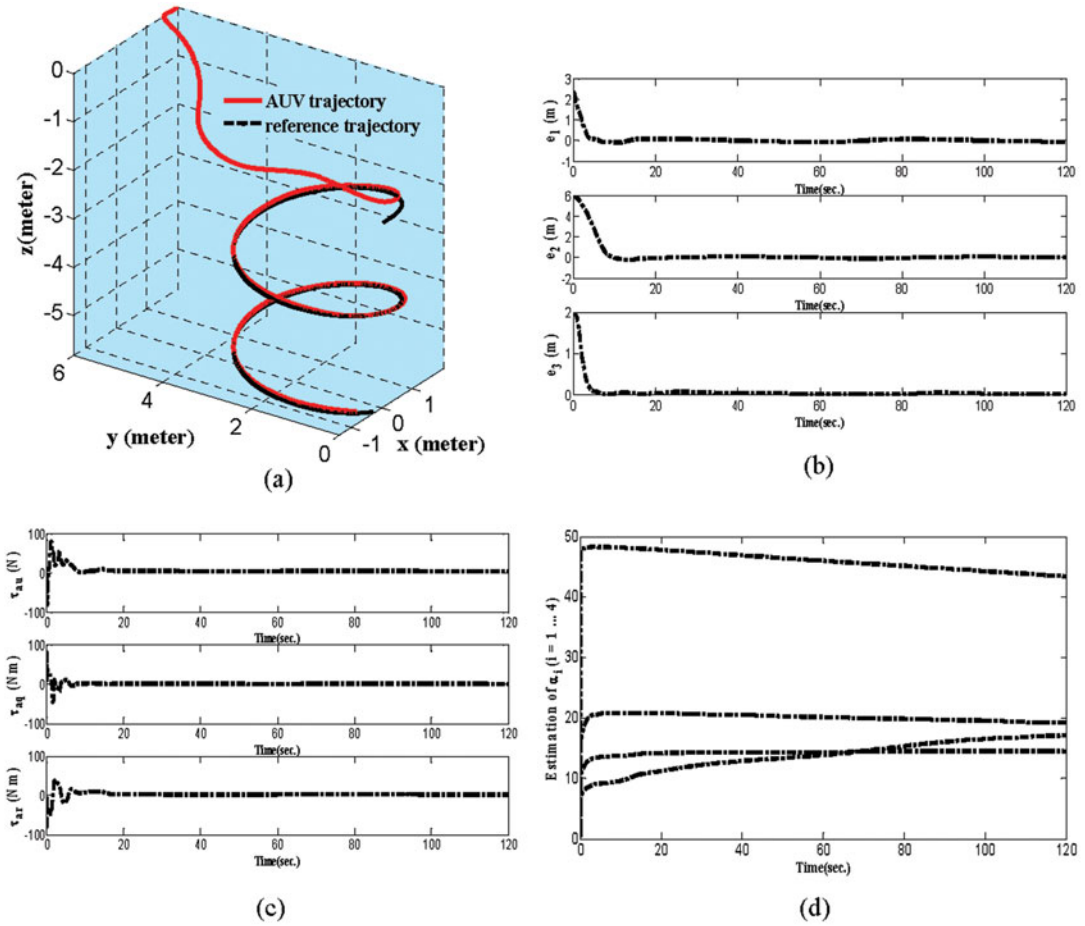

Fig. 4. Trajectory tracking results: (a) x–y–z plot, (b) output tracking errors, (c) control signals and (d) estimated parameters for the proposed controller.

is set to $x_d(0) = 0\,\text{m}$, $y_d(0) = 0\,\text{m}$, $z_d(0) = -30\,\text{m}$, $\theta_d(0) = 0$ rad, and $\psi_d(0) = 0$ rad and $\varepsilon_t = 10$ is selected to reduce the chattering of the control signals. The results are illustrated in Fig. 5. It is obvious that the proposed controller performs better than the PD controller from the viewpoint of the feasible control signals. However, the PD controller surpasses in the final tracking accuracy at the expense of the actuator saturation and a chattering in the control signals. Figure 5(c) illustrates the output tracking errors in a logarithmic scale to show the final tracking accuracy clearly. The following *performance index* is used to evaluate the amount of the *control efforts* for each controller:

$$rms(\tau_{aj}(t)) = \sqrt{(1/T_f)\int_0^{T_f} \left|\tau_{aj}(t)\right|^2 dt}, \quad j = 1,\ 2,\ 3 \tag{59}$$

where T_f denotes the total running time and $\tau_{aj}(t)$ represents j-th element of the control input. The results are reported as $rms(\tau_{a1}(t)) = 130$, $rms(\tau_{a2}(t)) = 40$, and $rms(\tau_{a3}(t)) = 53$ for the proposed controller and $rms(\tau_{a1}(t)) = 235$, $rms(\tau_{a2}(t)) = 163$, and $rms(\tau_{a3}(t)) = 172$ for the PD controller. To evaluate the final tracking accuracy during the last T_L seconds, the performance index $e_{f,j} = \max_{T_f - T_L \le t \le T_f}\{|e_j(t)|\}$, $j = 1, 2, 3$ is used with $T_L = 5$sec. The results are reported as $e_{f,1} = 0.01\,\text{m}$, $e_{f,2} = 0.02\,\text{m}$, and $e_{f,3} = 0.06\,\text{m}$ for the proposed controller and $e_{f,1} = 0.004\,\text{m}$, $e_{f,2} = 0.001\,\text{m}$, and $e_{f,3} = 0.001\,\text{m}$ for the PD controller. As a consequence, the PD controller achieves a better final tracking accuracy at the expense of the large control efforts and unwanted chattering. Another simulation has been carried out which shows that the roughness of the PD control signals increases when the AUV starts from a very distant position relative to the desired trajectory. This leads to a poor transient performance. This result is illustrated by Fig. 6 for $x_d(0) = 0\,\text{m}$, $y_d(0) = 0\,\text{m}$,

https://doi.org/10.1017/S0263574717000455 Published online by Cambridge University Press

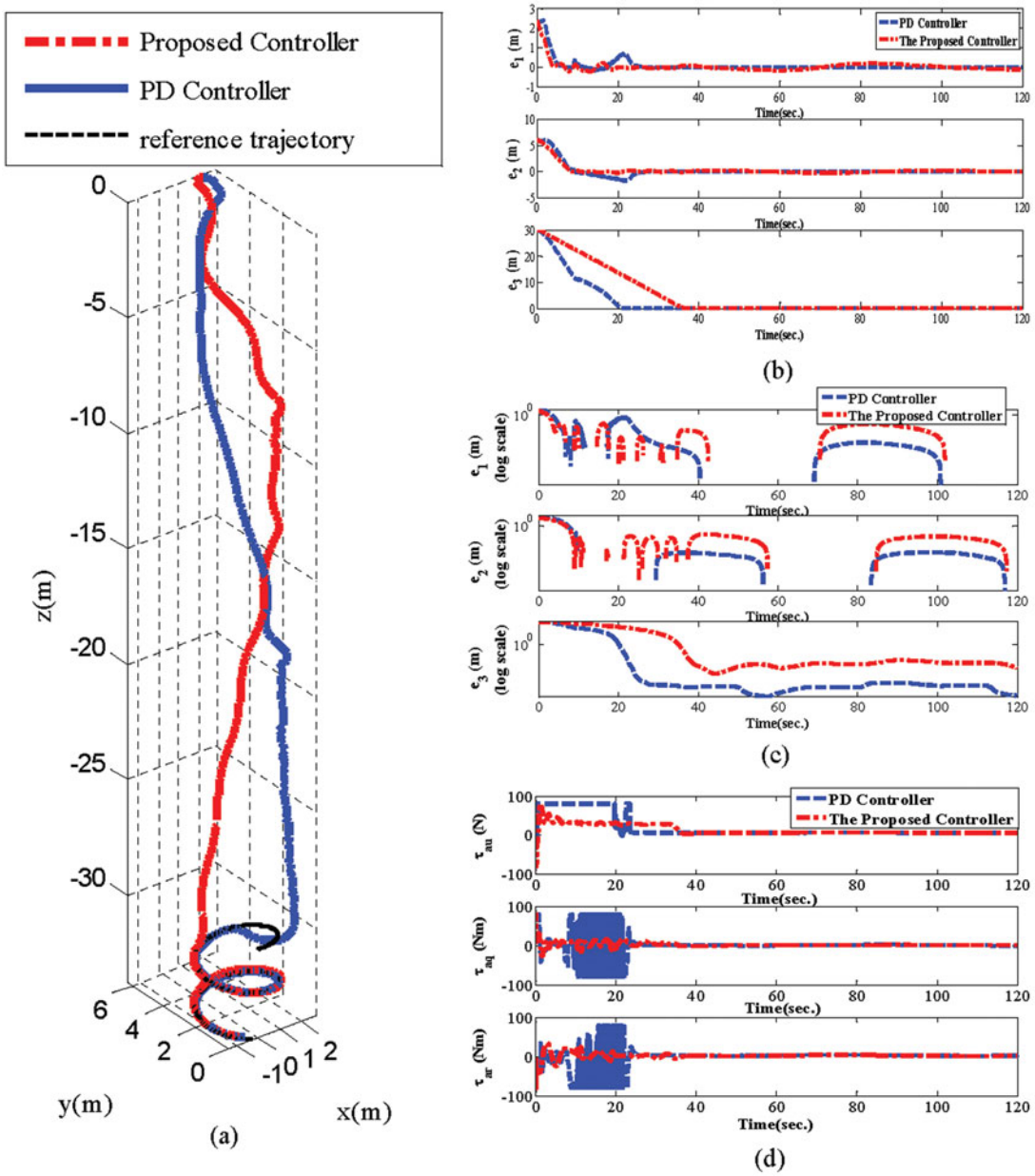

Fig. 5. Trajectory tracking results for the proposed and PD controllers: (a) x–y–z plot, (b) output tracking errors (linear scale), (c) output tracking errors (logarithmic scale) and (d) control signals.

$z_d(0) = -100\,\text{m}$, $\theta_d(0) = 0$ rad, and $\psi_d(0) = 0$ rad. It should be noted that the control signals are omitted in Fig. 6 because of a severe chattering.

A clear advantage of the proposed control system is the smoothness of the control signals. From a practical viewpoint, this feature shows that the generated control signals are acceptable by the AUVs actuators by considering their limited bandwidth. Therefore, the presented simulation results confirm the effectiveness of the proposed control system for a real implementation in offshore applications.

4.3. Controller robustness

In this section, the controller robustness and its stability are evaluated in the presence of the different levels of the uncertainties during the tracking mission. Since the controller employs an adaptive robust control strategy in the last term of (21), the controller effectively compensates all parametric and non-parametric uncertainties. If the level of the uncertainty increases due to the waves and ocean currents for example, the controller robustness is preserved at the expense of a larger adaptive gain and

https://doi.org/10.1017/S0263574717000455 Published online by Cambridge University Press

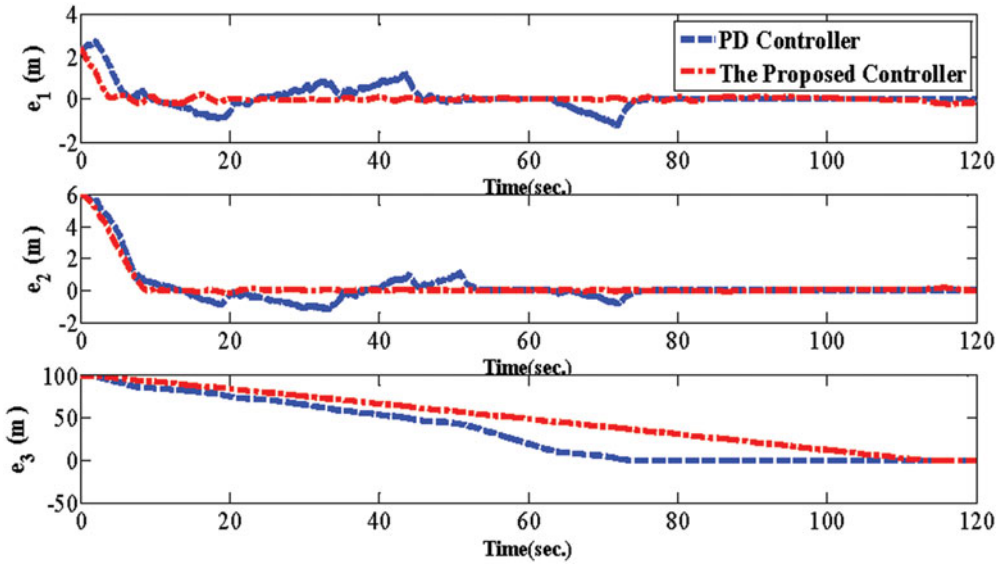

Fig. 6. The output tracking errors for the proposed and PD controllers for large initial tracking errors.

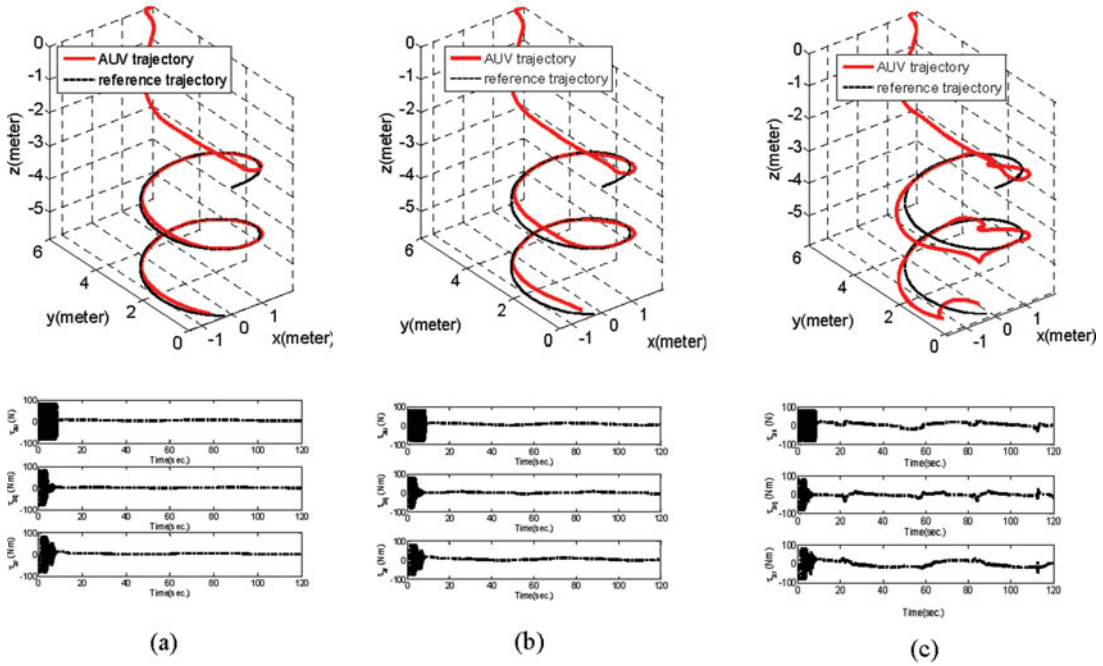

Fig. 7. Trajectory tracking results for different levels of uncertainties: (a) $A_f = 1$, $A_d = 2$, (b) $A_f = 2.5$, $A_d = 5$, (c) and $A_f = 5$, $A_d = 10$.

more chattering in the control signals. For a very high level of uncertainties, the chattering increases remarkably such that the control signals are not tolerable and feasible for the AUV actuators. Of course, this chattering can be decreased by choosing a larger value for ε_t at the expense of a less accuracy as stated in Remark 6. By further increasing of the uncertainties, the controller performance is extremely degraded and, finally, the controller stability may be lost. Figure 7 illustrates simulation results for ($A_f = 1$, $A_d = 2$), ($A_f = 2.5$, $A_d = 5$) and ($A_f = 5$, $A_d = 10$). As it is clear from this figure, the controller robustness is gradually degraded by increasing the level of the disturbances. Simulation results show that very high levels of the uncertainties greatly jeopardize the controller stability. As expressed above, the user may partly recover the tracking performance by increasing the adaptive gain $\mathbf{\Gamma}$ and the parameter ε_t. However, the controller robustness will be improved by

https://doi.org/10.1017/S0263574717000455 Published online by Cambridge University Press

redesigning the proposed controller with an effective combination of the neural networks and adaptive robust techniques. This subject is not in the scope of this paper.

5. Conclusion

In this paper, the OFB tracking control problem of the underactuated AUV subjected to the model uncertainties and input constraints has been addressed. The theoretical results have been presented to solve the 3D position control of AUVs when (i) the actuators are restricted to provide a limited amount of the torque inputs for the propellers; (ii) the velocity sensors are not available to supply the velocity measurements and (iii) the AUV parameters are not known and AUV suffers from environmental disturbances induced by the waves and ocean currents. The closed-loop stability of the proposed control system has been analyzed by Lyapunov's direct method. The presented stability analysis has shown that the closed-loop error variables are SGUUB. Finally, the simulation results have successfully verified the validity of the theoretical results. An extension of the proposed controller to the 3D OFB formation control of multiple AUVs with input constraints is devoted to the future works.

Acknowledgment

The author would like to thank the journal editor and anonymous reviewers for their valuable comments and suggestions which effectively improved the quality of the original manuscript. This research work was supported by research and technology program funded by Najafabad branch, Islamic Azad University under grant number 51504920613004 under the research project "Designing tracking controllers for the navigation of autonomous ocean vessels with limited information."

References

1. J. Yuh, "Design and control of autonomous underwater robots: A survey," *Autonoumous Robot.* **8**, 7–24 (2000).
2. Y. Nakamura and S. Savant, "Nonlinear Tracking Control of Autonomous Underwater Vehicle," *Proceedings of 1992 IEEE International Conference on Robotics and Automation*, Nice, France (1992) pp. A4–A9.
3. O. Egeland, M. Dalsmo and O. J. Sordalen, "Feedback control of a nonholonomic underwater vehicle with constant desired configuration," *Int. J. Robot. Res.* **15**(1), pp. 24–35 (1996).
4. N. E. Leonard, "Control synthesis and adaptation for an underactuated autonomous underwater vehicle," *IEEE J. Ocean. Eng.* **20**(3), 211–220 (1995).
5. K. Y. Pettersen and O. Egeland, "Time-varying exponential stabilization of the position and attitude of an underactuated autonomous underwater vehicle," *IEEE Trans. Autom. Control* **44**(1), 112–115 (1999).
6. Z. Md. Zain, K. Watanabe, K. Izumi and I. Nagai, "A discontinuous exponential stabilization law for an underactuated X4-AUV," *J. Artif. Life Robot.* **17**, 463–469 (2013).
7. C. A. Woolsey and L. Techy, "Cross-track control of a slender, underactuated AUV using potential shaping," *J. Ocean. Eng.* **36**, 82–91 (2009).
8. P. Batista, C. Silvestre and P. Oliviera, "A sensor-based controller for homing of underactuated AUVs," *IEEE Trans. Robot.* **25**(3), 701–716 (2009).
9. H. Xinjing, L. Yibo, D. Fei and J. Shijiu, "Horizontal path following for underactuated AUV based on dynamic circle guidance," *Robotica* **35**, 876–891 (2015).
10. K. D. Do, J. Pan and Z. P. Jiang, "Robust and adaptive path following for underactuated autonomous underwater vehicles," *Ocean Eng*. **31**(16), 1967–1997 (2006).
11. A. P. Aguiar and A. M. Pascoal, "Dynamic positioning and way-point tracking of underactuated AUVs in the presence of ocean currents," *Int. J. Control*. **80**(7), 1092–1108 (2007).
12. F. Repoulias and E. Papadopoulos, "Planar trajectory planning and tracking control design for underactuated AUVs," *Ocean Eng*. **34**, 1650–1667 (2007).
13. F. Y. Bi, Y. J. Wei, J. Z. Zhang and W. Cao, "Position-tracking control of underactuated autonomous underwater vehicles in the presence of unknown ocean currents," *IET Control Theory and Appl*. **4**(11), 2369–2380 (2009).
14. K. D. Do, Z. P. Jiang, J. Pan and H. Nijmeijer, "A global output-feedback controller for stabilization and tracking of underactuated ODIN: A spherical underwater vehicle," *Automatica* **40**, 117–124 (2004).
15. J. E. Refsnes, A. J. Sorensen and K. Y. Pettersen, "Model-based output feedback control of slender-body underactuated AUVs: theory and experiments," *IEEE Trans. Control Syst. Technol.* **16**(5), 930–946 (2008).
16. B. Subudhi, K. Mukherjee and S. Ghosh, "A static output feedback control design for path following of autonomous underwater vehicle in vertical plane," *Ocean Eng*. 63, 72–76 (2013).

17. X. Qi and Z. Cai, Three-dimensional formation control based on filter backstepping method for multiple underactuated underwater vehicles. *Robotica* 1–22 (2016). doi:10.1017/S0263574716000436.
18. B. Wehbe, S. Bazzi and E. Shammas, "Novel three-dimensional optimal path planning method for vehicles with constrained pitch and yaw," *Robotica* 1–20 (2016). doi:10.1017/S026357471600076X.
19. K. Shojaei and M. M. Arefi, "On the neuro-adaptive feedback linearizing control of underactuated autonomous underwater vehicles in three-dimensional space," *IET Control Theory Appl*. **9**(8), 1264–1273 (2015).
20. C. P. Bechlioulis, G. C. Karras, S. Heshmati-Alamdari and K. J. Kyriakopoulos, "Trajectory tracking with prescribed performance for underactuated underwater vehicles under model uncertainties and external disturbances," *IEEE Trans. Control Syst. Technol.* **25**(2), 429–440 (2017).
21. K. D. Do and J. Pan, *Control of Ships and Underwater Vehicles: Design for Underactuated and Nonlinear Marine Systems* (Springer, London, 2009).
22. T. I. Fossen, *Marine Control Systems* (Marine Cybernetics, Trondheim, Norway, 2002).
23. SNAME, the society of naval architects and marine engineers, "Nomenclature for treating the motion of a submerged body through a fluid," *Tech. Res. Bull.* 1–5 (1950).
24. K. Shojaei and M. Dolatshahi, "Line-of-sight target tracking control of underactuated autonomous underwater vehicles," *Ocean Eng*. **133**, 244–252 (2017).
25. J. H. Li, P. M. Lee, B. H. Jun and Y. K. Lim, "Point-to-point navigation of underactuated ships," *Automatica* **44**(12), 3201–3205 (2008).
26. F. L. Lewis, D. M. Dawson and C. T. Abdallah, *Robot Manipulator Control Theory and Practice*, 2nd ed. (Marcel Dekker Inc., New York, 2004).
27. E. Aguinaga-Ruiz, A. Zavala-Rio, V. Santibanez and F. Reyes, "Global trajectory tracking through static feedback for robot manipulators with bounded inputs," *IEEE Trans. Control Syst. Technol.* **17**(4), 934–944 (2009).
28. M. M. Polycarpou, "Stable adaptive neural control scheme for nonlinear systems," *IEEE Trans. Autom. Control* **41**, 447–451 (1996).
29. H. Berghuis and H. Nijmeijer, "A passivity approach to controller-observer design for robots," *IEEE Trans. Robot. Autom.* **9**(6), 740–754 (1993).
30. M. A. Arteaga and R. Kelly, "Robot control without velocity measurements: New theory and experimental results," *IEEE Trans. Robot. Autom.* **20**(2), 297–308 (2004).